ADJUSTMENT IN NUMERICAL WEATHER PREDICTION MODELS IN THE TROPICS

W. A. Heckley
ECMWF

1. INTRODUCTION

The analysis-forecasting system at ECMWF is a highly integrated scheme. Analyses are performed four times daily 00Z, 06Z, 12Z and 18Z. A six hour forecast is made from each of these analyses to provide a 'first guess' for the subsequent analysis. Thus the analysis may be thought of as, in some sense, continuous. In addition, a ten day forecast is run from the 12Z analysis, each day.

An analysis is many things to many people and it is important to question the role of the analysis in an analysis-forecasting system. For observational studies it is clear that an analysis should represent as accurately as possible the actual structure of the atmosphere; it is not so clear that this is true, or even desirable, if the analysis is to be used as an initial data set from which a forecast is to be made. As an example, if the analysis is influenced by processes that the numerical model is unable (through inadequate physics, perhaps) to describe, the model will attempt to interpret these aspects of the analysis in terms of its own physics, which implies that the model's physical forcing will be wrong. Any imbalance remaining will excite spurious high frequency inertia-gravity oscillations which may have large amplitude. In order to minimise the effect of these oscillations on the forecast, a non-linear normal mode initialisation is employed to zero the time tendency of these modes. Unfortunately, until very recently this initialisation was adiabatic, thus in the tropics, where diabatic forcing is dominant, the divergence field was considerably weakened. If the model is to have the correct forcing for the processes it is able to describe, only these, and all these, processes must be represented in the analysis. In addition, the mass/wind balance of this analysis must be sufficiently good as to exclude spurious large amplitude inertia-gravity oscillations. This is rather a strong statement and in practice it is obvious that it is more important for certain processes than for others. The problem essentially revolves around interpretation of observations. As one would expect, the problem is prominent in the tropics where the combination of relatively poor model physics, poor interpretation of data and sparse data coverage can result in large changes to the first guess field which often produce unrealistic structures.

In Section 2 some examples of this adjustment in the tropics will be given for March and April, 1981. These months have not been chosen for any à priori reason; other months have been investigated and similar conclusions can be drawn. Section 3 describes some simple theoretical ideas related to this problem.

2. SOME EXAMPLES OF ADJUSTMENT IN THE TROPICS

2.1 Changes in the divergent flow

Fig. 1 shows ensemble means of the March, 1981 velocity potential fields at 1000 mb for (a) the 12Z uninitialised analyses, (b) the 12Z initialised analyses, (c) the 24 hour forecasts, and (d) the 240 hour forecasts. Over most of the tropics the velocity potential field has been slightly weakened by the initialisation. The most noticeable difference occurs over the western Pacific, Indonesian region where there has been a weakening of the divergent circulation. As the initialisation is only applied to the first five vertical modes, features with a small vertical scale in the lower troposphere should be unaffected. The velocity potential at 1000 and 850 mb is largely a product of Ekman pumping in the PBL and therefore, due to the small vertical extent of the PBL, will be largely unchanged by the initialisation. The larger (vertical) scale convectively driven features will be removed by the initialisation as the initialisation procedure did not at this time include diabatic processes. Thus the changes in the velocity potential field in the western Pacific, Indonesian region are most likely due to failure of the initialisation procedure to retain the observed large-scale convective circulations. By 24 hours the divergent circulation has increased slightly in intensity and, apart from one or two notable exceptions, is very similar to the uninitialised analysis. The divergent circulation in the western Pacific, Indonesian region, removed by the initialisation, has returned with almost its original magnitude, although the centre is slightly too far eastward. The notable exceptions are the African and, to a lesser extent, South American regions. In these regions the 24-hour forecast has substantially increased low level convergence relative to both the initialised and uninitialised analyses. In terms of the magnitude of the velocity potential the uninitialised analysis has a 3×10^{-6} s^{-1} contour over central Africa, while the 24-hour forecast has a 6×10^{-6} s^{-1} contour. After the first 24 hours of the forecast the velocity potential in these regions decreases although even by 240 hours has a larger magnitude than the uninitialised analysis. The 240 hour forecast has some of the gross features of the analysis but is lacking in some important details.

The 850 mb velocity potential fields are shown in Fig. 2. At this level the initialisation has again had little influence. The main differences occur in the western Pacific, Indonesian region; other differences, such as a slackening of gradients over Colombia, can also be seen but are quite small. The 24-hour forecast velocity potential is generally more intense than the uninitialised analysis and dramatically so over the African region; this indicates very intense convergence. By 240 hours the velocity potential field has gradients not much larger than those of the uninitialised analysis.

The 200 mb fields are shown in Fig. 3. The initialised analysis has all the features of the uninitialised analysis but, as expected, is much weaker in the

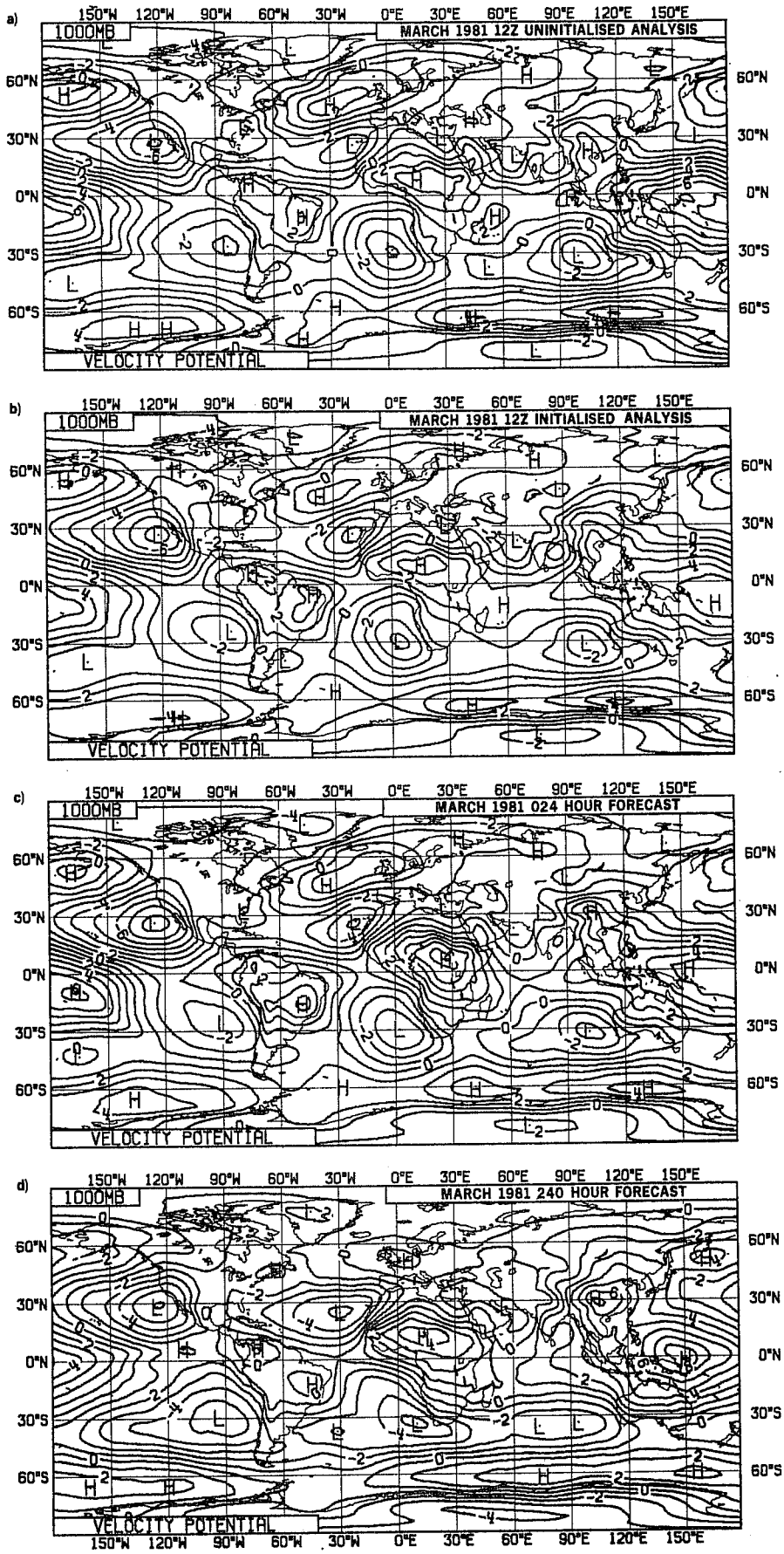

Fig. 1 1000 mb velocity potential fields of the ensemble mean March 1981 fields. Contour interval $10^{-6}s^{-1}$. (a) 12Z uninitialised analysis. (b) 12Z initialised analysis. (c) 24 hour forecast. (d) 240 hour forecast.

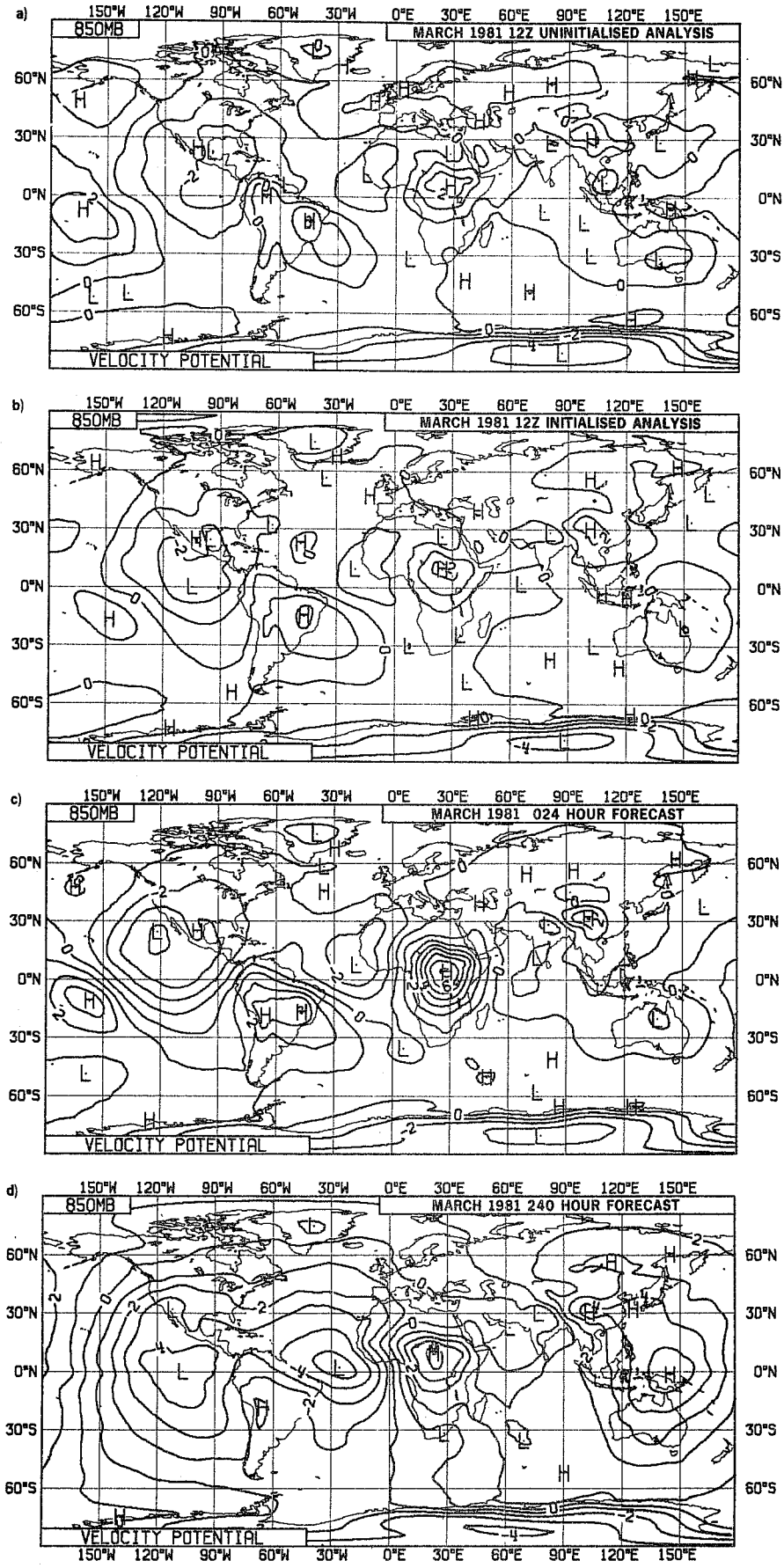

Fig. 2 As Fig. 1 but for 850 mb.

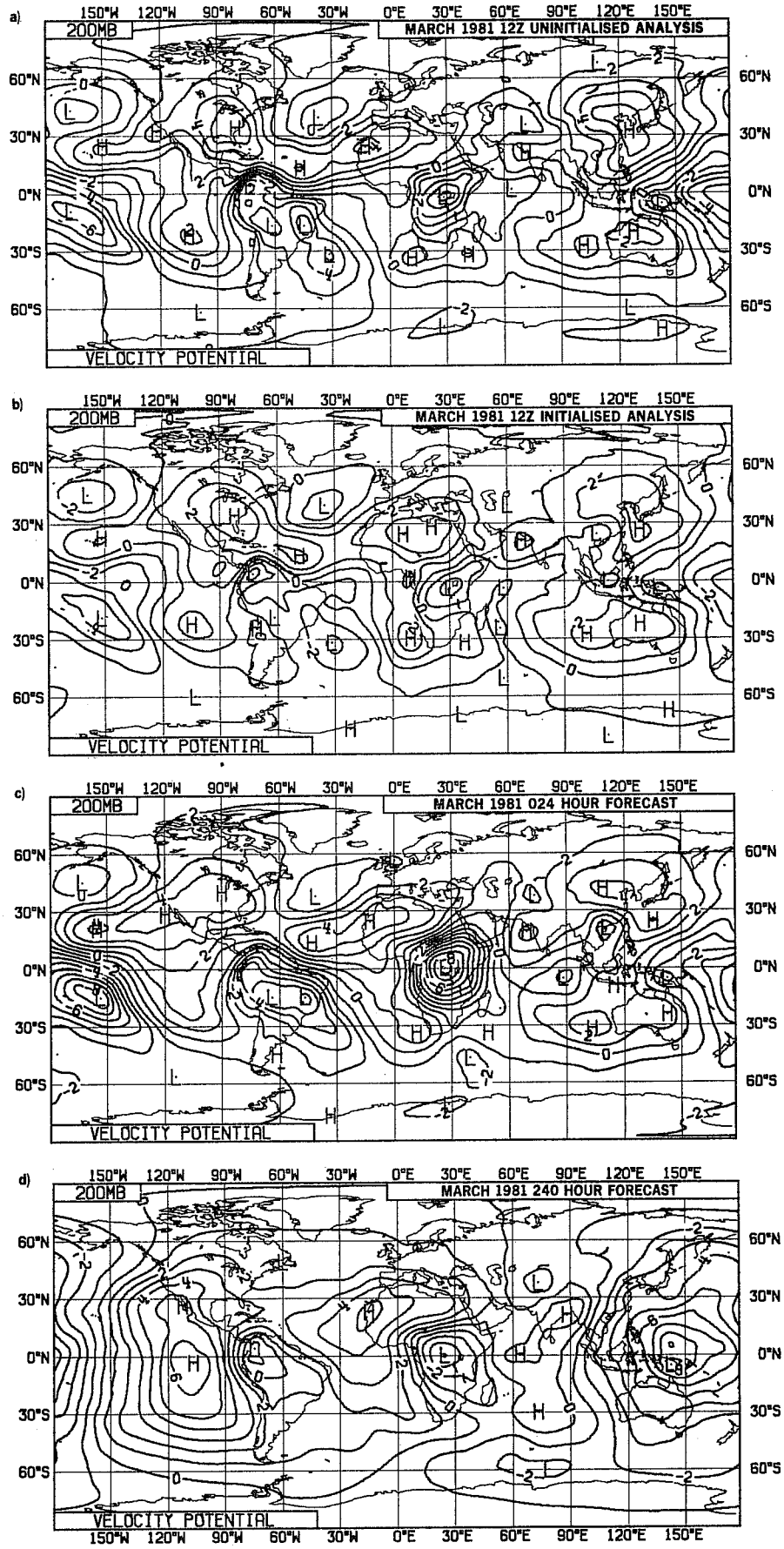

Fig. 3 As Fig. 1 but for 200 mb.

tropics. Again, the most significant difference between the 24-hour forecast and the uninitialised analysis is the enormous intensification of the velocity potential over the African region, corresponding at this level to intense divergence. The intensity of gradients in the 240 hour forecast are closer to the uninitialised analysis than earlier in the forecast but are badly located, particularly over the Pacific.

2.2 Changes in the wind field during the initialisation and first 24 hours of the forecast

Although it is common practice to concentrate on the 200 mb level, the changes are slightly larger at 150 mb, therefore, for clarity, the figures will concentrate on this level. Fig. 4 shows the ensemble mean 12Z, uninitialised, analysed wind field, in the African region, for April, 1981 for (a) 150 mb and (b) 850 mb. At 150 mb there are westerly jets north and south of the equator; the northern hemisphere jet has wind speeds of up to 43 ms^{-1} and the southern hemisphere jet of up to 31 ms^{-1}. Nearer the equator the flow is generally westerly, but much weaker and with appreciable northerly cross equatorial flow. At 850 mb the flow is generally easterly of typically 6 to 8 ms^{-1}; some southerly cross-equatorial flow is evident.

The effect of initialisation on the analysis is illustrated in Fig. 5, which shows wind field of the ensemble mean 12Z uninitialised analysis minus the ensemble mean 12Z initialised analysis for April, 1981, for (a) 150 mb and (b) 850 mb. Comparing Fig. 5(a) and 5(b) it is clear that the initialisation changes are as large at 850 mb as they are at 150 mb, typically 2 or 3 ms^{-1}. Although, as can be seen from Figs. 6(a) and 6(b), the changes at 150 mb are almost entirely within the divergent component while those at 850 mb are almost entirely within the rotational component. This is not to imply that the initialisation changes the rotational component of the flow, the initialisation changes the surface pressure which effectively moves the 850 mb level for example to a different part of the flow, where the rotational component may be different. The 150 mb changes correspond to a weakening of the large scale divergent circulation over Africa, largely as a result of the exclusion of diabatic forcing in the initialisation procedure. The 850 mb changes are largely a result of surface pressure changes in the initialisation due to barotropic mass/wind imbalances in the uninitialised analysis. From Figs. 4 and 5 it is clear that the changes at 150 mb represent a much smaller fraction of the total wind than do those at 850 mb which suggests that the cause of the mass/wind imbalance in the uninitialised analysis is probably a relatively more serious problem than the absence of diabatic forcing in the initialisation procedure.

Fig. 7 shows the mean error in the wind field at (a) 150 mb and (b) 850 mb given by the monthly mean 24-hour forecast minus the monthly mean initialised analysis, for April, 1981. A very similar pattern can be seen in other months and in individual forecasts. The wind field errors over the South American region also have a similar pattern but are weaker. Broadly, this erroneous flow consists, at 850 mb,

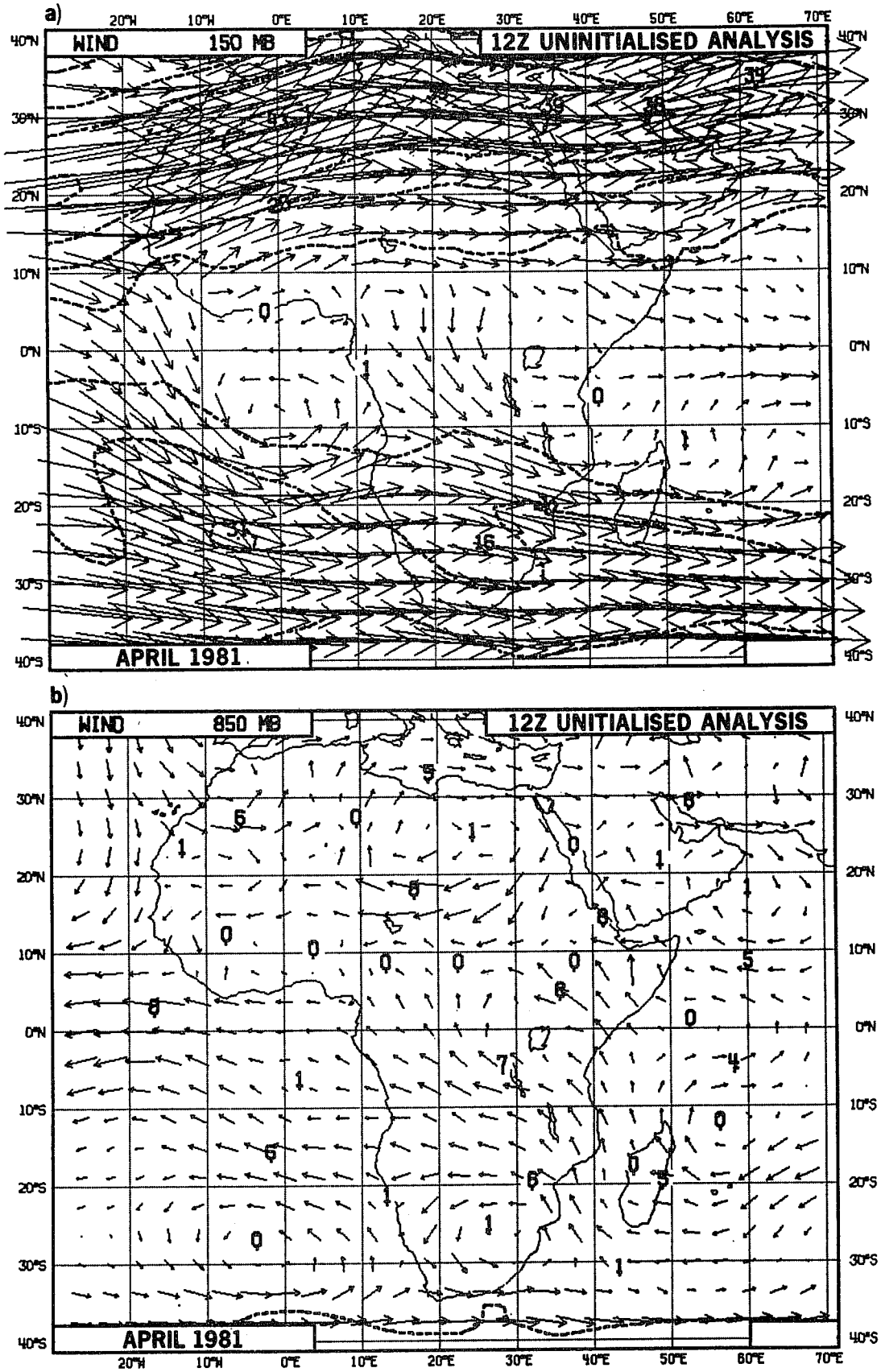

Fig. 4 Vector wind field of the ensemble mean April 1981 12Z initialised analysis (a) 150 mb. (b) 850 mb.

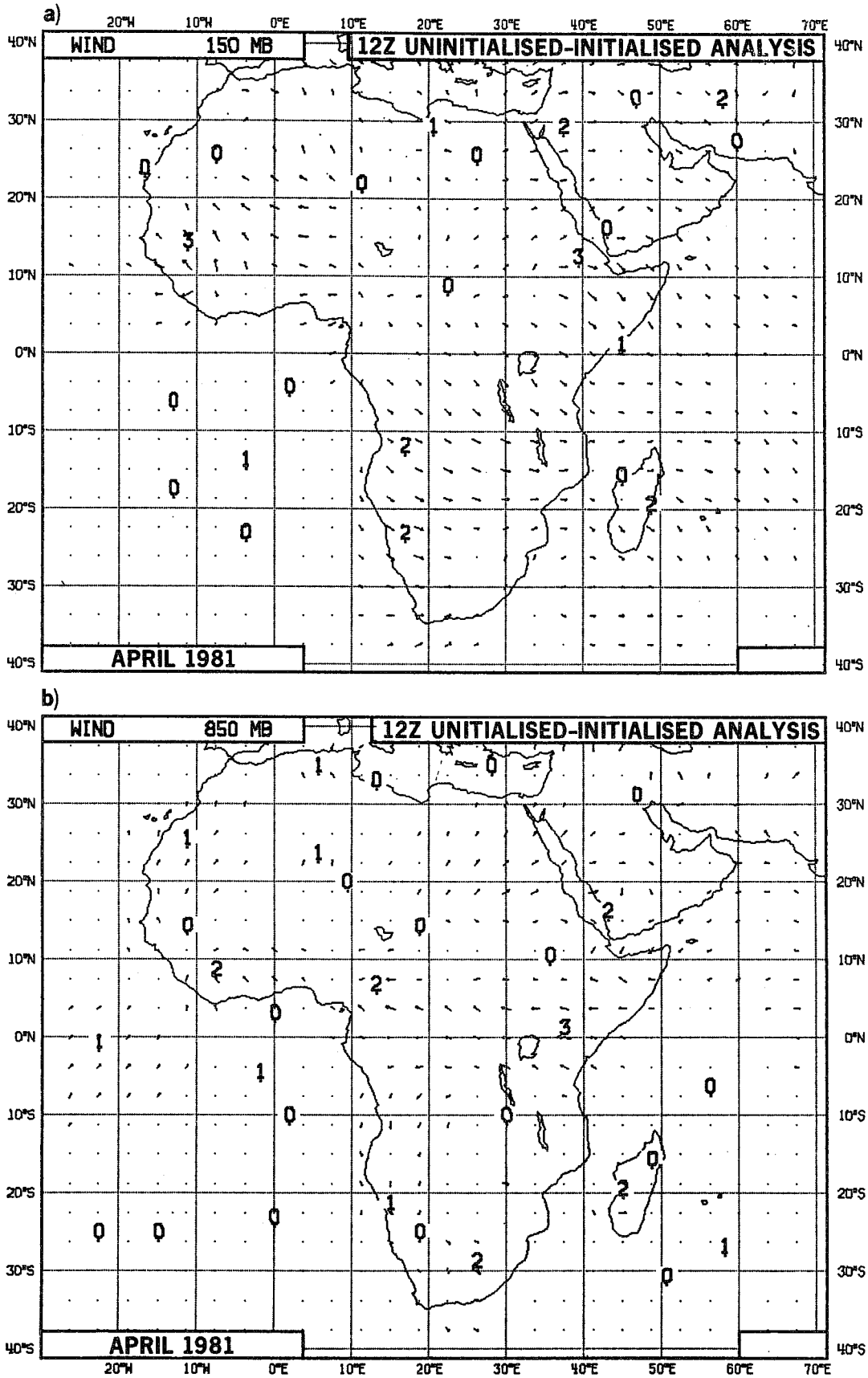

Fig. 5 Vector wind field of the ensemble mean 12Z uninitialised analysis minus the ensemble mean 12Z initialised analysis for April 1981. (a) 150 mb. (b) 850 mb.

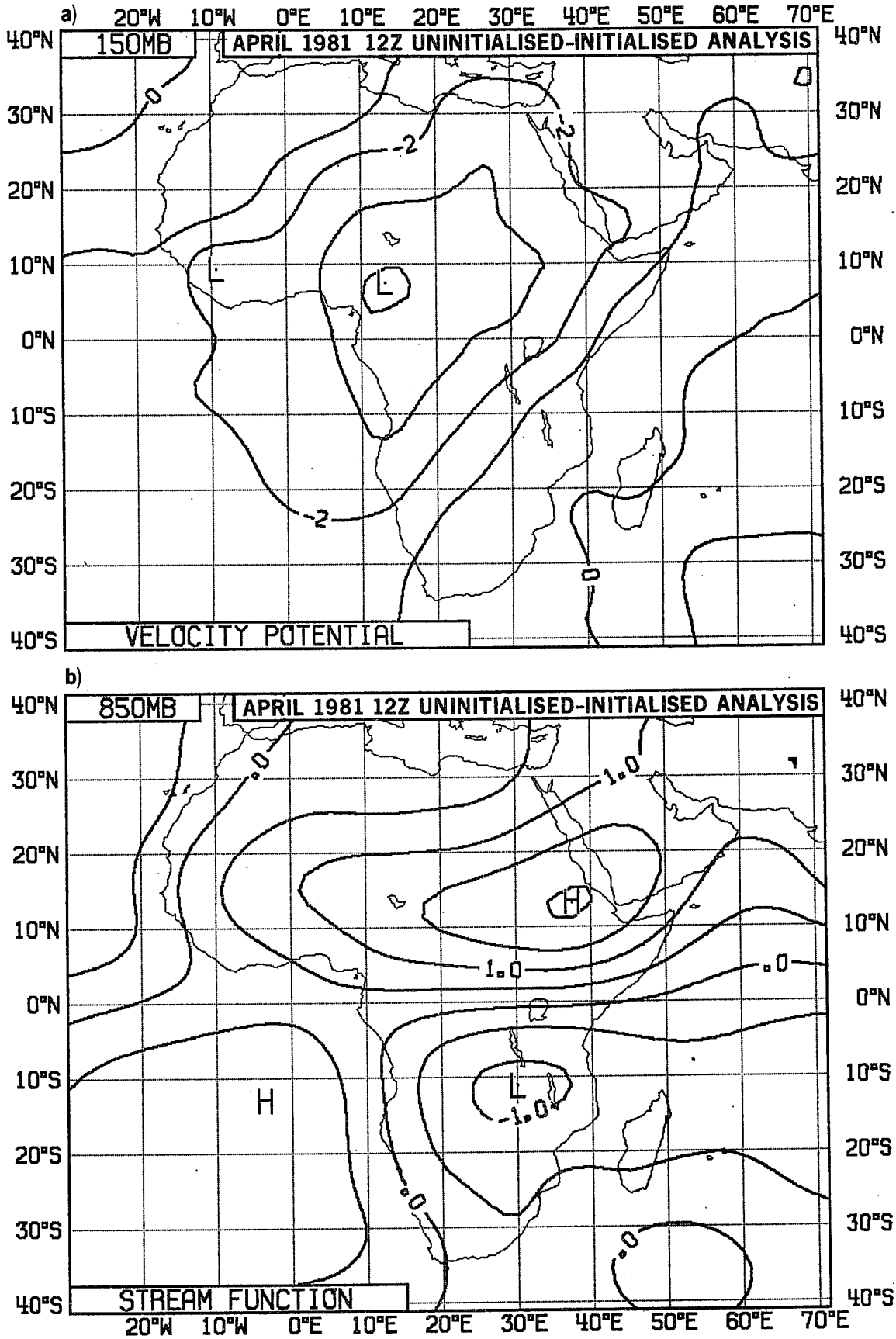

Fig. 6 Ensemble mean 12Z uninitialised analysis minus the ensemble mean 12Z initialised analysis, for April 1981. Contouring interval $10^{-6}s^{-1}$. (a) The 150 mb velocity potential. (b) The 850 mb stream function.

of westerlies off west Africa, easterlies off east Africa and cyclonic flow over north and south Africa. The 150 mb flow is the reverse of this with easterlies off west Africa, westerlies off east Africa and anti-cyclonic flow over north and south Africa. There are errors in the mean 24 hour forecast of up to 11 ms^{-1} at 150 mb and up to 7 ms^{-1} at 850 mb. The associated velocity potential fields are shown in Fig. 8(a) for 150 mb and Fig. 8(b) for 850 mb, these indicate large erroneous low level convergence and upper level divergence.

It is interesting to project these changes onto the normal modes of the model. Fig. 9 shows the contributibution to the error field at 150 mb of the first five vertical modes, zonal wavenumbers up to 20 and meridional wavenumbers up to 39 for (a) the Rossby modes (includes the mixed Rossby gravity mode) and (b) the inertia-gravity modes. Fig. 10 shows the contributions of these modes at 850 mb. Comparing Figs. 9 and 10 with Fig. 7 it is clear that these modes account for most of the error field at 150 mb, but at 850 mb the higher vertical modes make an appreciable contribution. Most of the large errors are accounted for by the contributions of these modes with the Rossby modes contributing slightly more than the gravity modes.

Fig. 11 shows the contribution to the error field at 150 mb of the first five vertical modes, zonal wavenumbers up to 20 but only the gravest symmetric plus the gravest asymmetric meridional modes for (a) the Rossby modes and (b) the gravity modes. Comparing with Fig. 9 it is apparent that about 80% of the gravity wave response occurs in these gravest meridional modes while the higher meridional index Rossby modes make a substantial contribution.

The situation is similar at 850 mb (Fig. 12) where, again, the higher meridional index Rossby modes are relatively more important than the higher meridional index inertia-gravity modes.

On these scales the inertia-gravity modes are almost entirely divergent while the Rossby modes are almost entirely rotational; most of the changes in the velocity potential are accounted for by the inertia-gravity modes. Fig. 13 shows the velocity potential field associated with the inertia-gravity mode contributions to the error field, of the first five vertical modes, zonal wavenumbers up to 20 and the gravest symmetric plus the gravest asymmetric modes, for (a) 150 mb and (b) 850 mb. Comparing with the total changes shown in Fig. 8 we see that these modes account for just over half of the total changes. A further 25% or so is accounted for by the higher meridional index inertia-gravity modes, the remainder is accounted for by higher vertical modes and contributions from from the Rossby modes.

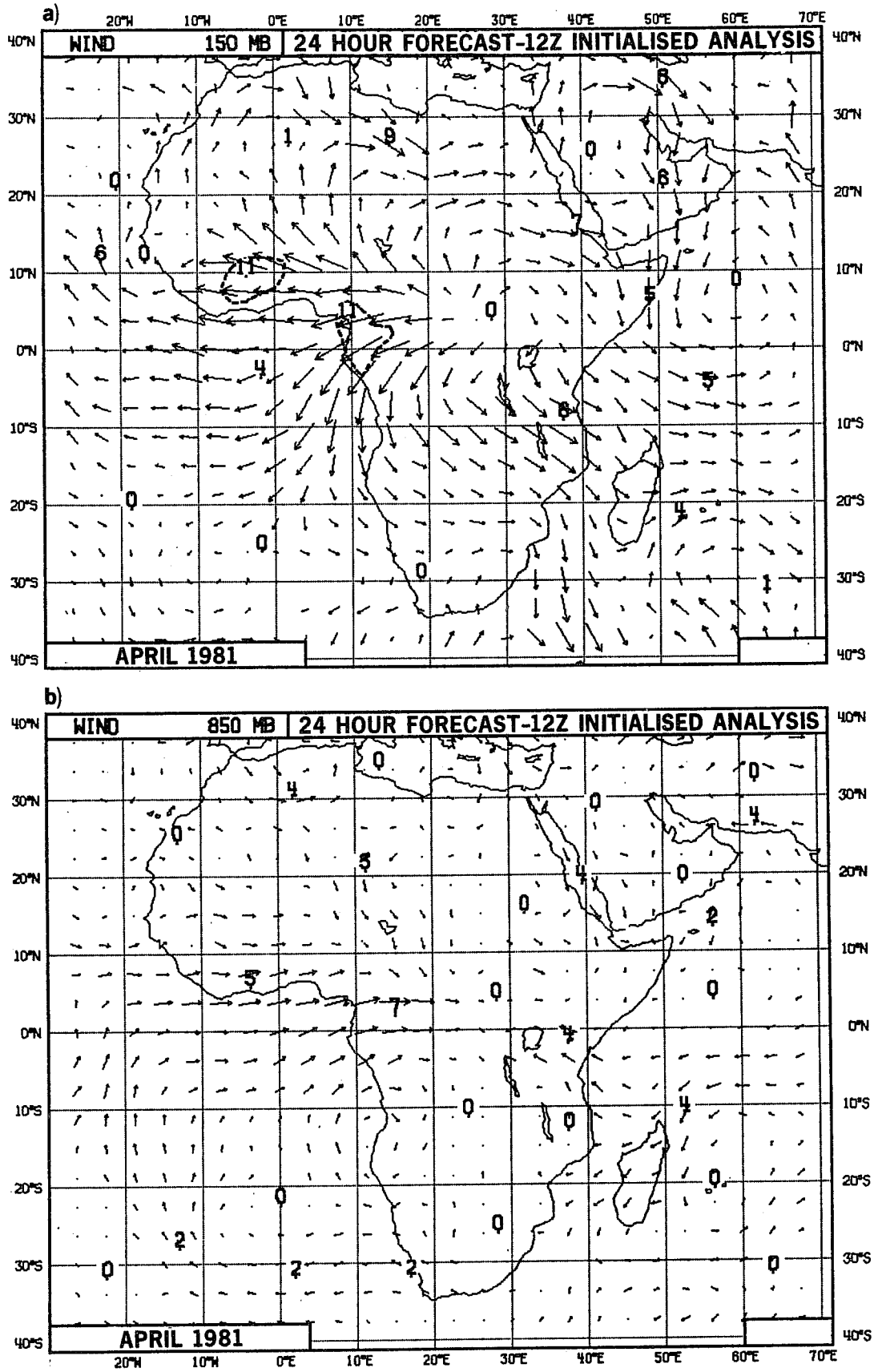

Fig. 7 Vector wind field of the ensemble mean 24 hour forecast minus the ensemble mean 12Z initialised analysis, for April 1981. (a) 150 mb. (b) 850 mb.

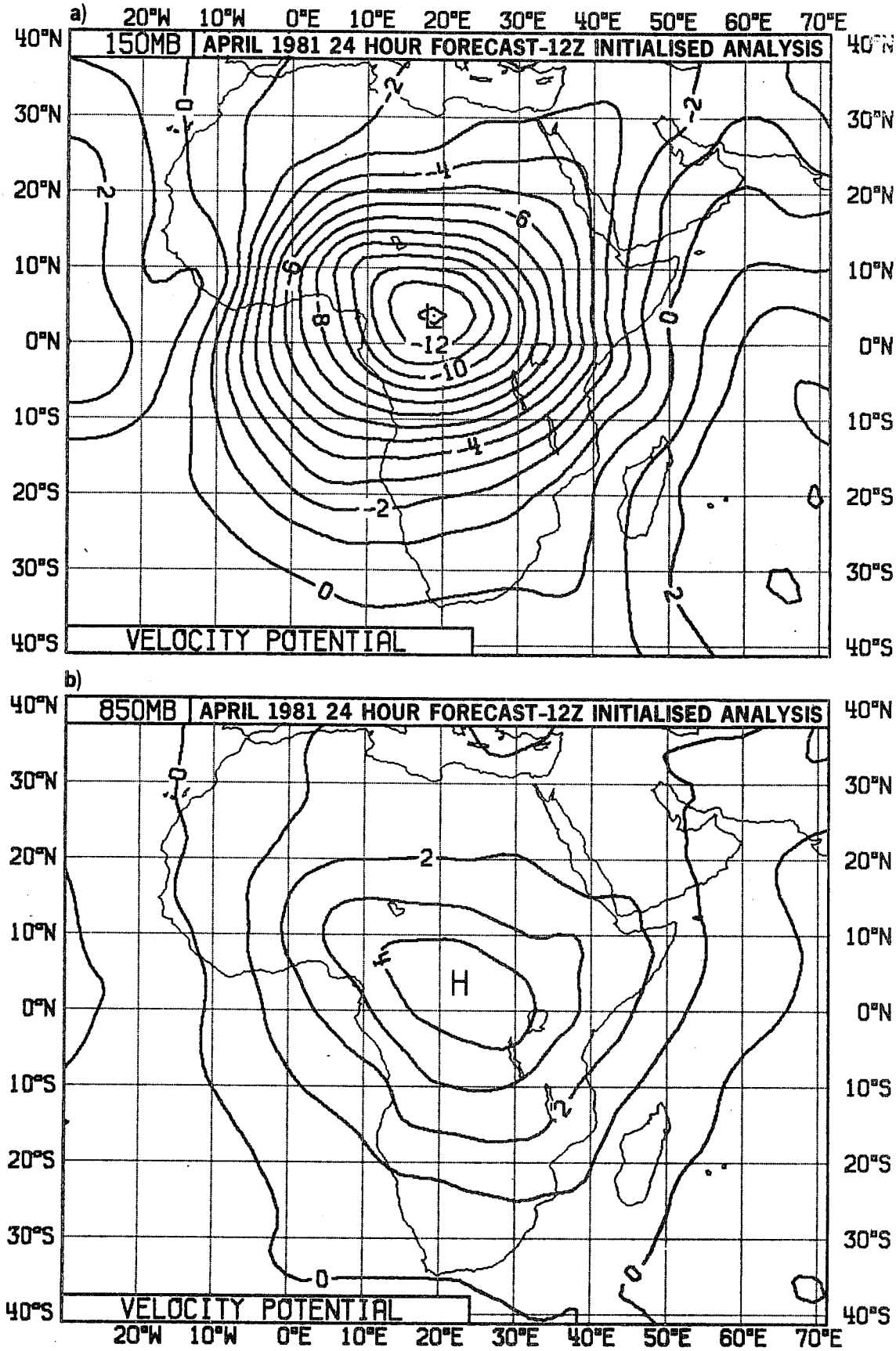

Fig. 8 As Fig. 7 but for the velocity potential, contouring interval $10^{-6}s^{-1}$.

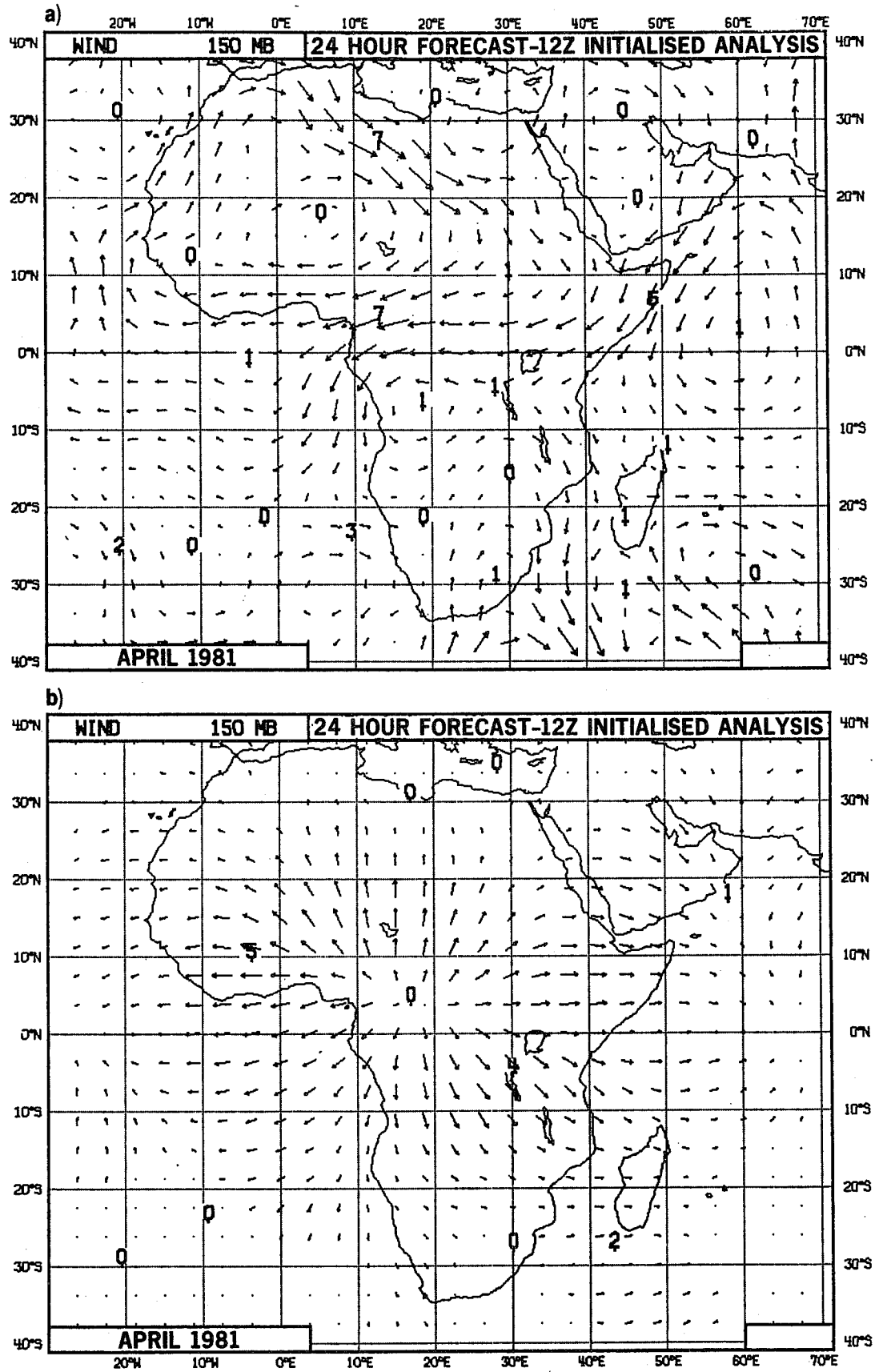

Fig. 9 Ensemble mean 24 hour forecast minus the ensemble mean 12Z initialised analysis, for April 1981. The vector wind field at 150 mb, composed of the first five vertical modes, zonal wavenumbers up to 20 and meridional modes up to 39. (a) The Rossby modes (includes the mixed Rossby-gravity mode). (b) The inertia-gravity modes.

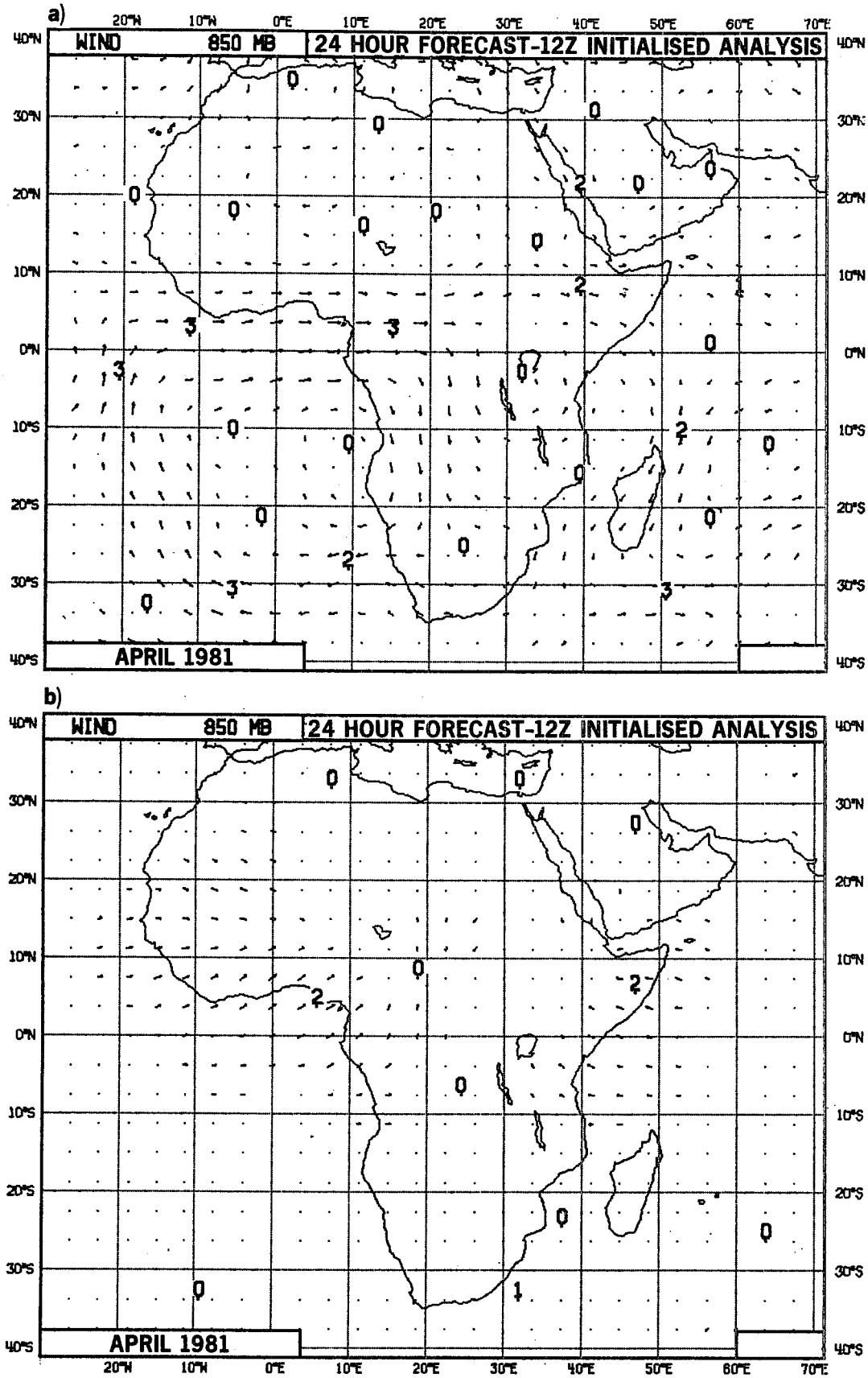

Fig. 10 As Fig. 9 but for 850 mb.

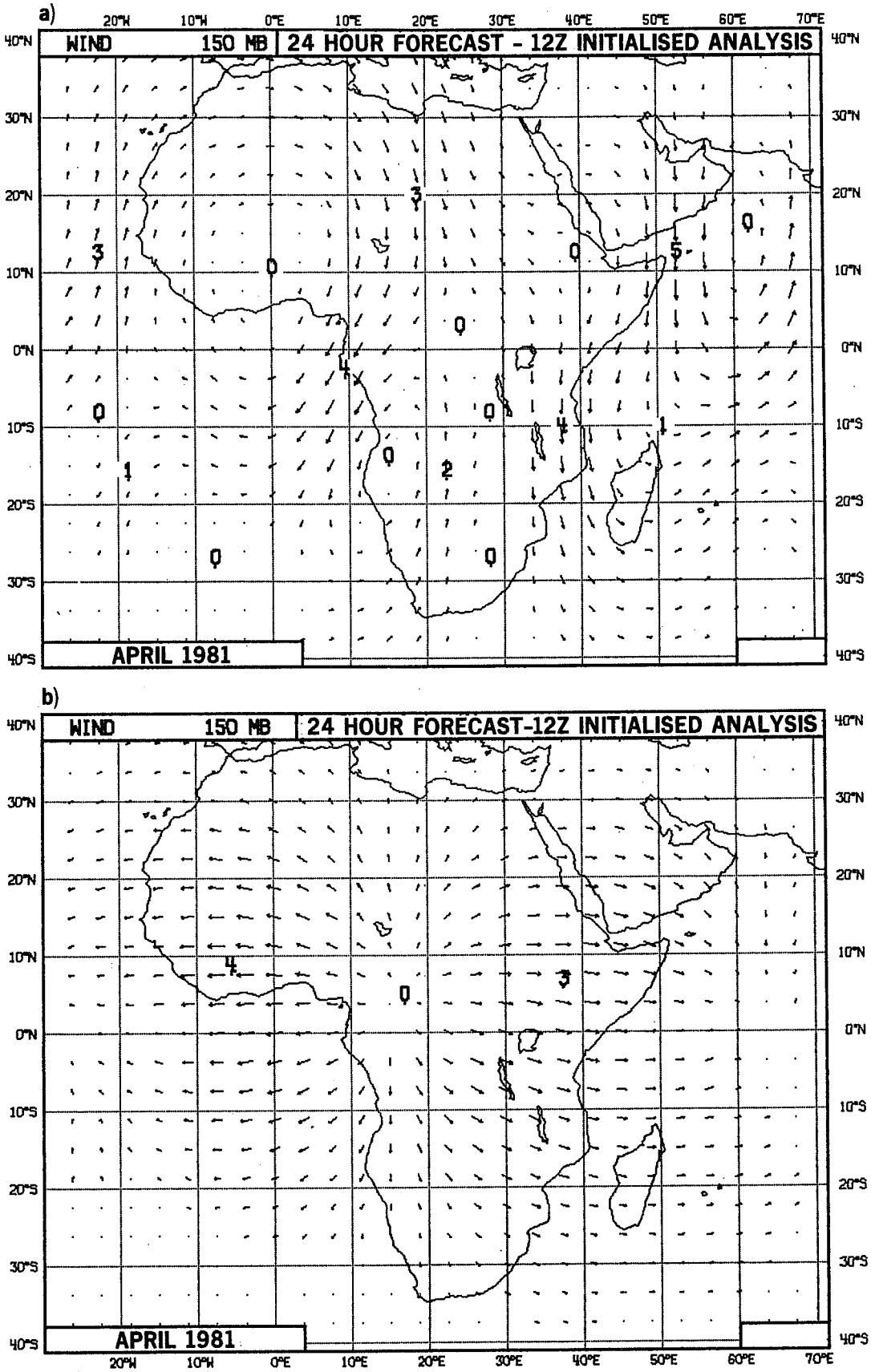

Fig. 11 As Fig. 9 but only the gravest symmetric plus the gravest asymmetric meridional modes.

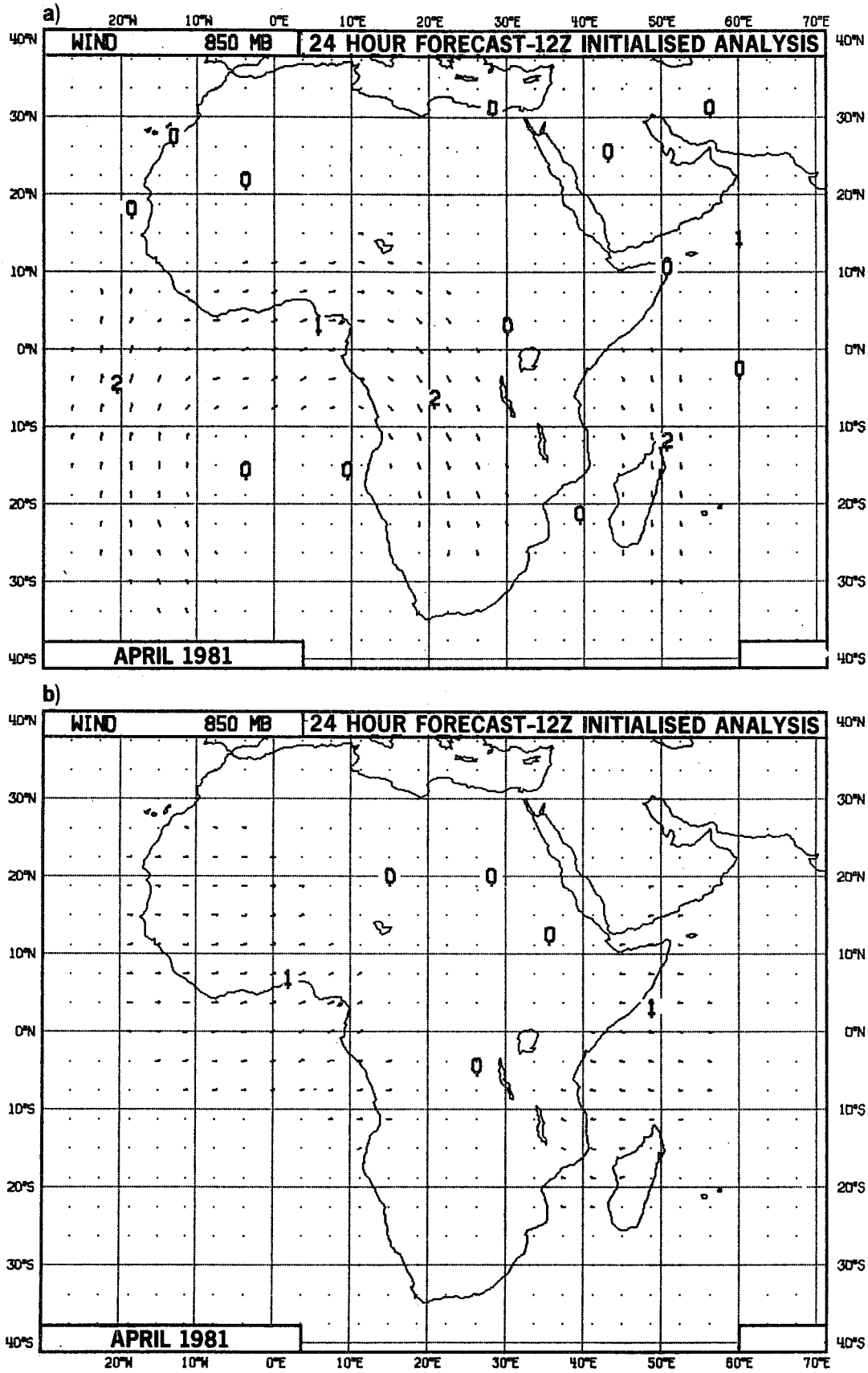

Fig. 12 As Fig. 11 but for 850 mb.

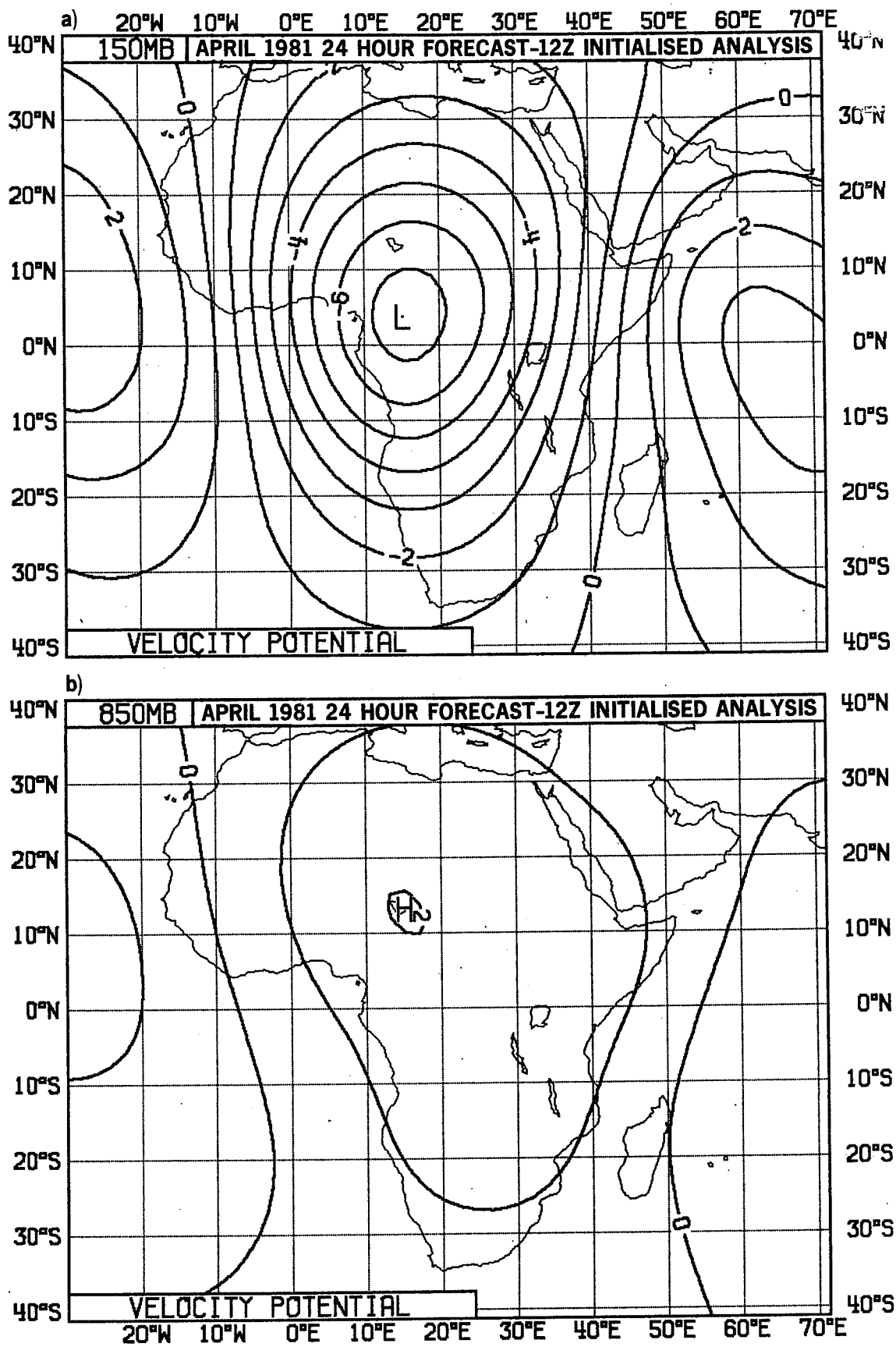

Fig. 13 Ensemble mean 24 hour forecast minus the ensemble mean 12Z initialised analysis for April 1981. The velocity potential field associated with inertia-gravity modes composed of the first five vertical modes, zonal wavenumbers up to 20 and the gravest symmetric plus the gravest asymmetric modes. (a) 150 mb. (b) 850 mb.

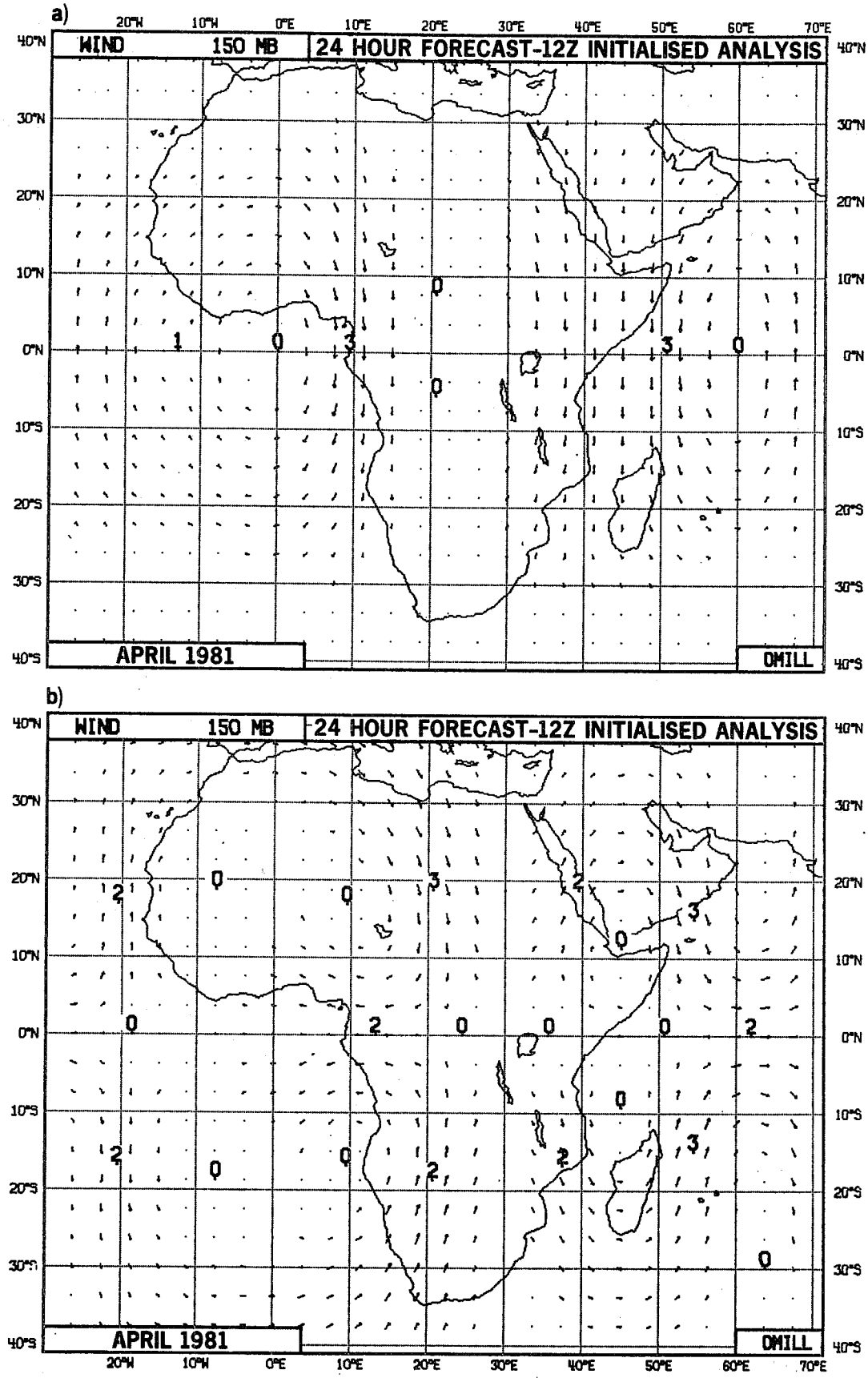

Fig. 14 Ensemble mean 24 hour forecast minus the ensemble mean 12Z initialised analysis, for April 1981. The vector wind field at 150 mb composed of the first five vertical modes and zonal wavenumbers up to 20. (a) The gravest meridional asymmetric Rossby wave (the mixed Rossby-gravity wave). (b) The gravest meridional symmetric Rossby wave.

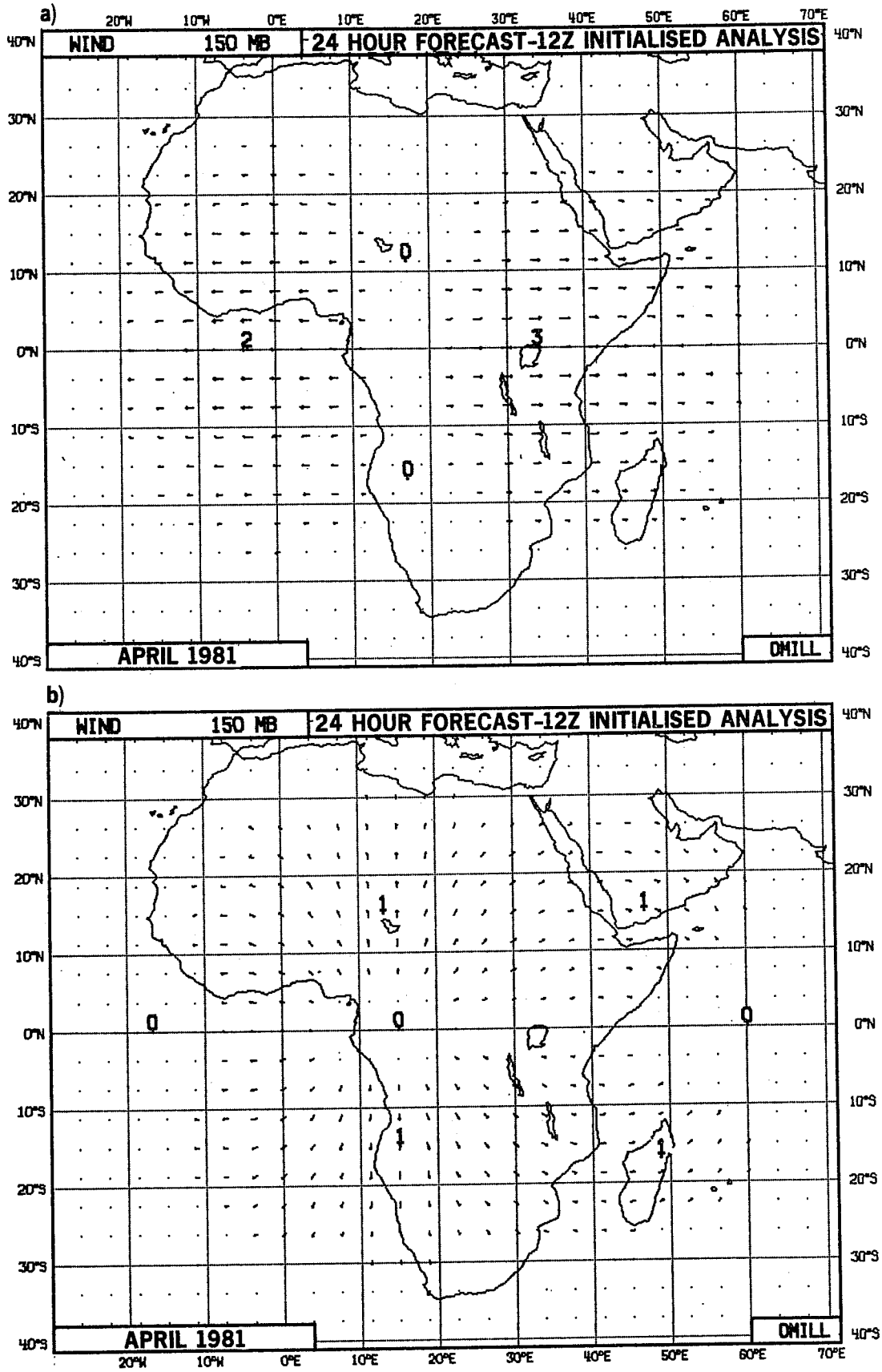

Fig. 15 As Fig. 14 but for (a) The eastward propagating gravest meridional symmetric inertia-gravity mode (the Kelvin mode). (b) The westward propagating gravest meridional symmetric inertia-gravity mode.

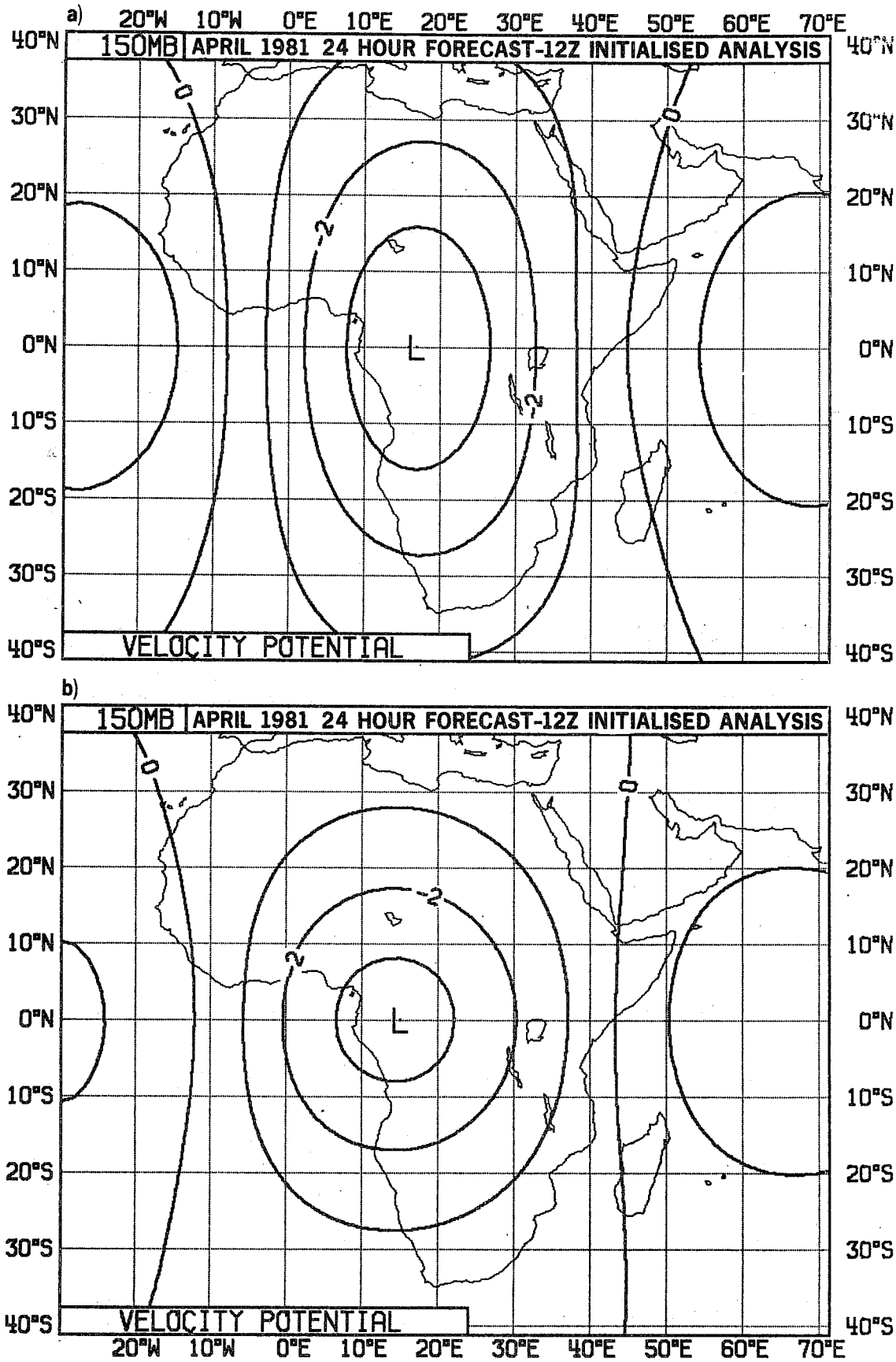

Fig. 16 As Fig. 15 but for velocity potential. Contouring interval $10^{-6}s^{-1}$.

Fig. 14 shows the contributions to the 150 mb, 24 hour, error field of (a) the gravest asymmetric Rossby wave (the mixed Rossby gravity wave), first five vertical modes, zonal wavenumbers up to 20; and (b) the gravest symmetric Rossby wave, first five vertical modes, zonal wavenumbers up to 20. These two modes contribute about equally, 2 or 3 ms^{-1} each.

Fig. 15 shows the contributions to the 150 mb, 24 hours, error field of (a) the eastward propagating gravest symmetric inertia-gravity mode (the Kelvin mode), first five vertical modes, zonal wavenumbers up to 20; and (b) the westward propagating gravest symmetric inertia-gravity mode, first five vertical modes, zonal wavenumbers up to 20. Fig. 16 shows the velocity potential of these contributions. The contribution of these two modes are similar, with that of the Kelvin mode being slightly larger. The eastward and westward propagating gravest asymmetric inertia-gravity mode contributions are very small.

Thus the 24-hour error field is dominated by contributions from four meridional modes: the Kelvin mode; the westward propagating gravest symmetric inertia-gravity mode; the mixed Rossby-gravity mode and the gravest symmetric Rossby mode. All these modes having roughly the same amplitude, the Rossby modes being largely rotational and the inertia-gravity modes being largely divergent. In addition to these modes contributions are made by the higher index meridional modes (notably Rossby modes) and, particularly at low levels, the higher vertical modes.

2.3 Changes in the wind field after the first 24 hours of the forecast

Fig. 17 shows the wind field associated with the difference between the ensemble mean 48 hour forecast and the ensemble mean 24 hour forecast for April 1981 for (a) 150 mb and (b) 850 mb. The field has some similarity with the 24-00 hour differences shown in Fig. 7 and the wind speeds are of similar magnitude. Of particular interest is the velocity potential associated with the field, shown in Fig. 18 for (a) 150 mb and (b) 850 mb. The changes in the velocity potential in the 48-24 hour fields are about half the magnitude of the changes in the 24-00 hour fields but they are in the opposite sense, indicating changes in the sense of low level divergence and upper level convergence, and there is a shift westward of the pattern. Although the amplitude of the inertia-gravity wave changes in the 48-24 hour period are about half of those during the 24-00 hour period, the amplitude of the Rossby wave changes are about the same. After 48 hours the inertia-gravity modes change very little, however the Rossby modes continue to change for, on average, 7 to 8 days into the forecast.

In terms of differences with respect to the initialised analysis the first 24 hours of the forecast is characterised by a rapid development of low level

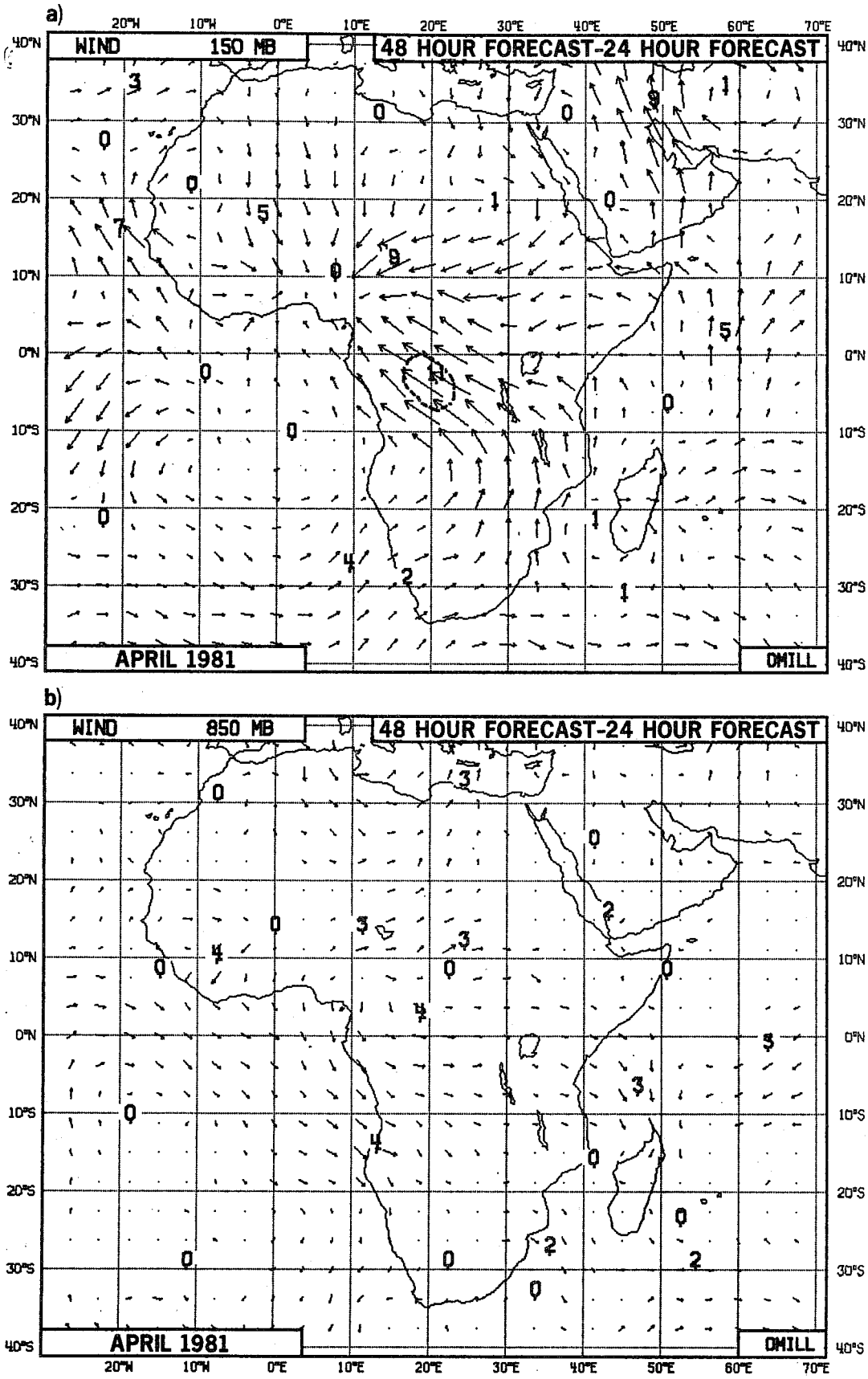

Fig. 17 Vector wind field of the ensemble mean 48 hour forecast minus the ensemble mean 24 hour forecast, for April 1981. (a) 150 mb. (b) 850 mb.

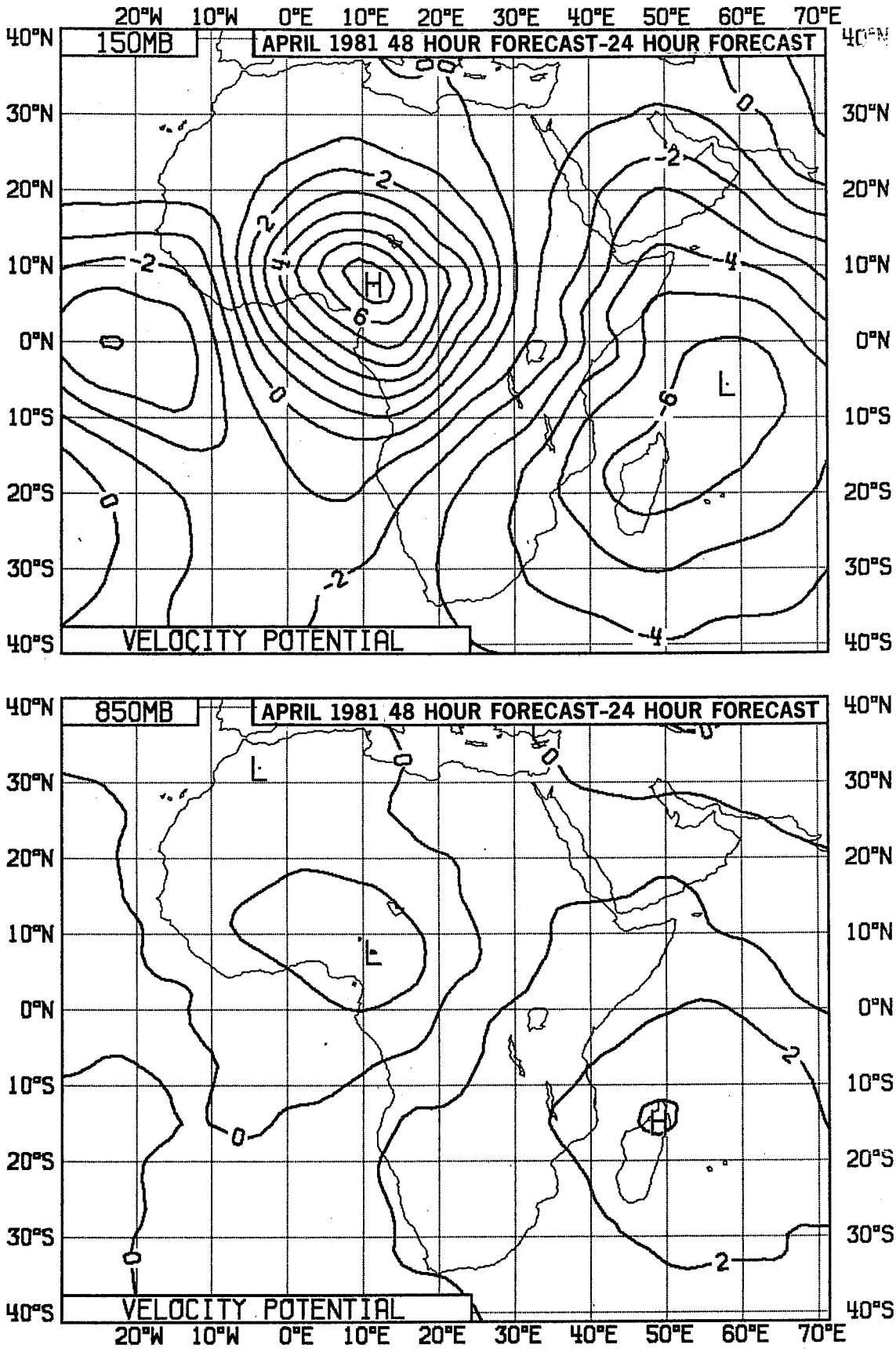

Fig. 18 As for Fig. 17 but for the velocity potential, contouring interval $10^{-6}s^{-1}$.

convergence and upper level divergence over the tropical continents, principally Africa. This response then appears to 'overshoot', turning to upper level convergence during the second 24 hours of the forecast. Thereafter there is little change in the gravity wave amplitudes during the forecasts. Thus the 'adjustment' of the gravity waves takes, in the mean, one or two days. By contrast, the 'adjustment' of the Rossby waves takes, in the mean, 7 to 8 days.

3. SOME SIMPLE ANALYTICAL SOLUTIONS TO THE PROBLEM OF FORCED EQUATORIAL LONG WAVES

3.1 Applicability of the solutions

This section describes some simple time-dependent analytical solutions to the problem of a sudden 'switch-on' of localised heating, symmetric or asymmetric about the equator. In the present context the sudden switch-on of localised heating may be thought of as the start of a forecast from an initial data set which has, by reason of poor model physics or poor intepretation of data, a spurious local thermal source. The solutions described in this section would then, if the forecasting model were linear, describe the error growth in the forecasting model.

3.2 The model

As in Gill (1980), the aim is to study the response of the tropical atmosphere to a given distribution of heating using as simple a model as possible. The linearized shallow water equations on the β-plane are used in their non-dimensional form. These equations and the implied approximations are discussed in detail by Gill (1980). They have the form

$$\partial u/\partial t - \tfrac{1}{2}yv = -\partial p/\partial x \quad , \tag{2.1}$$

$$\partial v/\partial t + \tfrac{1}{2}yu = -\partial p/\partial y \quad , \tag{2.2}$$

$$\partial p/\partial t + \partial u/\partial x + \partial v/\partial y = -Q \quad . \tag{2.3}$$

where x is the non dimensional distance eastwards

y is the non dimensional distance north from the equator

(u,v) is proportional to horizontal velocity and p is proportional to the pressure perturbation. Q is proportional to the heating rate, the signs being such that if Q is positive, the signs of u,v,p correspond to those at the surface.

The length scale is the equatorial Rossby radius $(c/2\beta)^{\frac{1}{2}}$ and the time scale is $(2\beta c)^{-\frac{1}{2}}$ where $c = (gH)^{\frac{1}{2}}$. For an equivalent depth, H, of 400 m, the Rossby radius

is about 10^{o} latitude and the time scale is about one quarter of a day.

The vertical velocity is given by

$$w = \partial p/\partial t + Q \ . \qquad (2.4).$$

In order to simplify the problem still further the long wave approximation of assuming that the eastward flow is in geostrophic balance with the north-south pressure gradient will be made. As discussed in Hollingsworth and Simmons (1983), this eliminates the gravity waves. The term will also have a small effect on the long wave solutions.

This study is concerned with the transient response to a sudden 'switch-on' of heating at t=0 and the ensuing evolution of the flow towards steady state. In order to have a steady state, dissipative processes must be included. The most convenient form is "Rayleigh friction" and "Newtonian cooling" which replaces $\partial/\partial t$ by $\partial/\partial t+\varepsilon$. For simplicity, as in Gill (1980), it is assumed that the ε for friction is the same as that for cooling. The equations then take the form

$$\partial u/\partial t + \varepsilon u - \tfrac{1}{2} yv = -\partial p/\partial x \ , \qquad (2.5)$$

$$\tfrac{1}{2} yu = -\partial p/\partial y \ , \qquad (2.6)$$

$$\partial p/\partial t + \varepsilon p + \partial u/\partial x + \partial v/\partial y = - Q \ , \qquad (2.7)$$

$$w = \partial p/\partial t + \varepsilon p + Q. \qquad (2.8)$$

3.3 Method of solution

Defining the Laplace transform of a function f(t) as $\bar{f}(c) = \int_0^\infty f(t)e^{-ct}dt$ and taking the Laplace transforms of Eqns. (2.5) to (2.8), we obtain

$$c\bar{u} - u(o) + \varepsilon\bar{u} - \tfrac{1}{2}y\bar{v} = - \partial\bar{p}/\partial x \ , \qquad (3.1)$$

$$\tfrac{1}{2}y\bar{u} = - \partial\bar{p}/\partial y \ ; \qquad (3.2)$$

$$c\bar{p} - p(o) + \varepsilon\bar{p} + \partial\bar{u}/\partial x + \partial\bar{v}/\partial y = - \bar{Q} \ , \qquad (3.3)$$

$$\bar{w} = c\bar{p} - p(o) + \varepsilon\bar{p} + \bar{Q}. \qquad (3.4)$$

The unperturbed state consists of an atmosphere at rest with properties a function of z only, therefore

$$u(o) = p(o) = 0 \quad , \tag{3.5}$$

and (3.1) to (3.4) become

$$(c + \varepsilon)\bar{u} - \tfrac{1}{2}y\bar{v} = - \partial\bar{p}/\partial x \quad , \tag{3.6}$$

$$\tfrac{1}{2}y\bar{u} = - \partial\bar{p}/\partial y \quad , \tag{3.7}$$

$$(c + \varepsilon)\bar{p} + \partial\bar{u}/\partial x + \partial\bar{v}/\partial y = - \bar{Q} \quad , \tag{3.8}$$

$$\bar{w} = (c + \varepsilon)\bar{p} + \bar{Q}. \tag{3.9}$$

The method of solution of these transformed equations closely follows Gill's (1980) solution of the steady state equations.

Introducing two new variables $\bar{q}$ and $\bar{r}$ to replace $\bar{p}$ and $\bar{u}$,

$$\bar{q} = \bar{p} + \bar{u} \ , \tag{3.10}$$

$$\bar{r} = \bar{p} - \bar{u} \ , \tag{3.11}$$

The sum and difference of (3.8) and (3.6) yield

$$(c+\varepsilon)\bar{q} + \partial\bar{q}/\partial x + \partial\bar{v}/\partial y - \tfrac{1}{2}y\bar{v} = - \bar{Q} \quad , \tag{3.12}$$

$$(c+\varepsilon)\bar{r} - \partial\bar{r}/\partial x + \partial\bar{v}/\partial y + \tfrac{1}{2}y\bar{v} = - \bar{Q} \quad . \tag{3.13}$$

Eqn. (3.7) may be written as

$$\partial\bar{q}/\partial y + \tfrac{1}{2}y\bar{q} + \partial\bar{r}/\partial y - \tfrac{1}{2}y\bar{r} = 0 \quad . \tag{3.14}$$

The free solutions of (3.12), (3.13) and (3.14) have the form of parabolic cylinder functions $D_n(y)$ (Abramowitz and Stegun (1965), Ch. 19) and solutions

of the forced problem can be found by expanding the variables $\bar{q},\bar{r},\bar{v}$ and $\bar{Q}$ in terms of these functions. For example

$$\bar{q} = \sum_{n=0}^{\infty} \bar{q}_n(x)\, D_n(y) \ . \tag{3.15}$$

These have the properties

$$d\, D_n/dy + \tfrac{1}{2}y\, D_n = n\, D_{n-1} \ , \tag{3.16}$$

$$d\, D_n/dy - \tfrac{1}{2}y\, D_n = -\, D_{n+1} \ . \tag{3.17}$$

Substituting expressions of the form (3.15) into (3.12), (3.13) and (3.14), and using (3.16) and (3.17) gives

$$\left.\begin{aligned} (c+\varepsilon)\bar{q}_o + d\bar{q}_o/dx &= -\,\bar{Q}_o \\ (c+\varepsilon)\bar{q}_{n+1} + d\bar{q}_{n+1}/dx - \bar{v}_n &= -\,\bar{Q}_{n+1},\ n \geqslant 0 \end{aligned}\right\} \ , \tag{3.18}$$

$$(c+\varepsilon)\bar{r}_{n-1} - d\bar{r}_{n-1}/dx + n\bar{v}_n = -\,\bar{Q}_{n-1},\ n \geqslant 1 \ , \tag{3.19}$$

$$\left.\begin{aligned} \bar{q}_1 &= 0 \\ \bar{r}_{n-1} &= (n+1)\bar{q}_{n+1},\ n \geqslant 1 \end{aligned}\right\} \ . \tag{3.20}$$

In the following sections, solutions will be found for two special cases where the forcing has a particularly simple form. One is the case where the heating Q is symmetric about the equator and of the form

$$Q(x,y,t) = \begin{cases} 0 & , t < 0 \ , \\ F(x)\, D_o(y) = F(x)\, \exp(-\tfrac{1}{4}y^2) & , t > 0 \ . \end{cases} \tag{3.21}$$

which gives $\bar{Q}(x,y,c) = \frac{1}{c}\, F(x)\, \exp(-\tfrac{1}{4}y^2)$. (3.22)

The second has heating asymmetric about the equator and of the form

$$Q(x,y,t) = \begin{cases} 0 & , t < 0, \\ F(x)\, D_1(y) = F(x)y \exp(-\tfrac{1}{4}y^2), & t > 0. \end{cases} \tag{3.23}$$

which gives $\bar{Q}(x,y,c) = \frac{1}{c} F(x)y \exp(-\tfrac{1}{4}y^2)$. (3.24)

As pointed out by Gill (1980), these forms have the advantage that the response only involves parabolic cylinder functions up to order 3. These are given by

$$D_o, D_1, D_2, D_3 = (1, y, y^2-1, y^3-3y) \exp(-\tfrac{1}{4}y^2). \tag{3.25}$$

The forcing is assumed to be localised in the neighbourhood of x = 0 and to have the form

$$F(x) = \begin{cases} \cos(kx) & , |x| < L, \\ 0 & , |x| > L. \end{cases} \tag{3.26}$$

where $k = \pi/2L$ and L is taken as 2. (3.27)

This gives a heating region of latitudinal extent 2L, or about 40^o latitude, which is about the size of the convective region over Africa.

3.4 Symmetric forcing

The heating rate has the form of (3.21), the only non-zero coefficient $\bar{Q}_n$ is $\bar{Q}_o$ and is given by

$$\bar{Q}_o = 1/c\ F(x). \tag{4.1}$$

(a) The Kelvin wave part of the solution

There are two parts to the response to this form of forcing. The first part involved $\bar{q}_o$ only which satisfies (3.18) with n = 0. This solution represents the Kelvin wave which progresses eastwards. No information is carried westwards; the solution is zero for x < -L and so the solution of (3.18) is given by

$$\left.\begin{aligned}
&((c+\varepsilon)^2 + k^2)\bar{q}_o = 0 && , x < -L \\
&((c+\varepsilon)^2 + k^2)\bar{q}_o = -\frac{1}{c}\{(c+\varepsilon)\cos kx + k(\sin kx + \exp\{-(c+\varepsilon)(x+L)\})\} && , |x| < L \\
&((c+\varepsilon)^2 + k^2)\bar{q}_o = -\frac{k}{c}\{1 + \exp(-2(c+\varepsilon)L)\}\ \exp\{(c+\varepsilon)(L-x)\} && , x > L
\end{aligned}\right\} \quad (4.2)$$

Using (3.10), (3.11), (3.18) and (3.9) we may obtain expressions for the transformed variables $\bar{u}$, $\bar{p}$, $\bar{v}$ and $\bar{w}$.

$$\bar{u} \doteq \bar{p} = \tfrac{1}{2}\,\bar{q}_o(x,c)\ \exp(-\tfrac{1}{4}y^2) \quad , \qquad (4.3)$$

$$\bar{v} = 0 \quad , \qquad (4.4)$$

$$\bar{w} = \tfrac{1}{2}\{(c+\varepsilon)\bar{q}_o(x,c) + \frac{1}{c}F(x)\}\ \exp(-\tfrac{1}{4}y^2). \qquad (4.5)$$

The time dependent solution is obtained by taking the inverse Laplace transform of Eqns. (4.3) to (4.5). Those who are not interested in the details of the mathematical solution should skip to 3.4(b).

The inverse Laplace transform of $\bar{q}_o(x,c)$, which may be found by convoluting transforms of simple functions, is given by

$$\left.\begin{aligned}
&(\varepsilon^2 + k^2)q_o = 0 && , x < -L. \\
&(\varepsilon^2 + k^2)q_o = -\Big[\varepsilon\cos kx + k\sin kx - e^{-\varepsilon t}(\varepsilon\cos k(x-t) + k\sin k(x-t)) \\
&\qquad + \{ke^{-\varepsilon(x+L)} - e^{-\varepsilon t}(\varepsilon\sin k(t-(x+L)) + k\cos k(t-(x+L)))\}\ H(t-(x+L))\Big], \\
&\qquad\qquad |x| < L, \\
&(\varepsilon^2 + k^2)q_o = -\Big[\{ke^{-\varepsilon(x-L)} - e^{-\varepsilon t}(\varepsilon\sin k(t-(x-L)) + k\cos k(t-(x-L)))\}\ H(t-(x-L)) \\
&\qquad + \{ke^{-\varepsilon(x+L)} - e^{-\varepsilon t}(\varepsilon\sin k(t-(x+L)) + k\cos k(t-(x+L)))\}\ H(t-(x+L))\Big], \\
&\qquad\qquad x > L,
\end{aligned}\right\} \quad (4.6)$$

where 'H' is the Heaviside unit function.

In order to obtain an expression for w, it is necessary to find the inverse Laplace transform of $c\bar{q}_o(x,c)$. This may also be found by convoluting transforms of simple functions. It is given by

$$L^{-1}\{\bar{cq}_o\} = \begin{cases} 0 & , x < -L, \\ -e^{-\varepsilon t}\{\cos k(x-t) + \sin k(t-(x+L))\, H(t-(x+L))\} & , |x| < L, \\ -e^{-\varepsilon t}\{\sin k(t-(x-L))\, H(t-(x-L)) + \sin k(t-(x+L))\, H(t-(x+L))\}, & x > L. \end{cases} \tag{4.7}$$

Using (4.6) and (4.7), the solution becomes

$$u = p \begin{cases} = 0 & , x \le -L \\ = -\dfrac{\exp(-\frac{1}{4}y^2)}{2(\varepsilon^2+k^2)} \Big[\varepsilon \cos kx + k \sin kx - e^{-\varepsilon t}(\varepsilon \cos k(x-t) + k \sin k(x-t)) \\ \quad + \{ke^{-\varepsilon(x+L)} - e^{-\varepsilon t}(\varepsilon \sin k(t-(x+L)) + k \cos k(t-(x+L)))\}\, H(t-(x+L))\Big], \\ \qquad\qquad |x| < L, \\ = -\dfrac{\exp(-\frac{1}{4}y^2)}{2(\varepsilon^2+k^2)} \Big[\{ke^{-\varepsilon(x-L)} - e^{-\varepsilon t}(\varepsilon \sin k(t-(x-L)) + k \cos k(t-(x-L)))\} H(t-(x-L))\} \\ \quad + \{ke^{-\varepsilon(x+L)} - e^{-\varepsilon t}(\varepsilon \sin k(t-(x+L)) + k \cos k(t-(x+L)))\} H(t-(x+L))\} \\ \qquad\qquad x > L. \end{cases} \tag{4.8}$$

$$v = 0, \tag{4.9}$$

$$w \begin{cases} = 0 & , x < -L, \\ = \tfrac{1}{2}\exp(-\tfrac{1}{4}y^2)\Big\{\cos kx - \dfrac{1}{(\varepsilon^2+k^2)}\Big[\varepsilon^2 \cos kx + \varepsilon k \sin kx - ke^{-\varepsilon t}(\varepsilon \sin k(x-t) \\ \qquad - k \cos k(x-t)) \\ \quad + \{\varepsilon ke^{-\varepsilon(x+L)} - ke^{-\varepsilon t}(\varepsilon \cos k(t-(x+L)) - k \sin k(t-(x+L)))H(t-(x+L))\Big]\Big\} \\ \qquad\qquad , |x| < L, \\ = -\dfrac{\exp(-\frac{1}{4}y^2)}{2(\varepsilon^2+k^2)}\Big[\{\varepsilon ke^{-\varepsilon(x-L)} - ke^{-\varepsilon t}(\varepsilon \cos k(t-(x-L)) - k \sin k(t-(x-L)))\} \\ \qquad H(t-(x-L)) \\ \quad + \{\varepsilon ke^{-\varepsilon(x+L)} - ke^{-\varepsilon t}(\varepsilon \cos k(t-(x+L)) - k \sin k(t-(x+L)))\} \\ \qquad H(t-(x+L))\Big] \\ \qquad\qquad , x > L. \end{cases} \tag{4.10}$$

As expected, the solution represented by (4.8) to (4.10) tends towards Gill's (1980) steady state solution as $t \to \infty$.

(b) The planetary wave part of the solution

The second part of the forcing, which describes the mixed Rossby gravity wave, is obtained by putting n=1 in (3.18), (3.20) and (3.19), which then give

$$\bar{v}_1 = d\bar{q}_2/dx + (c+\varepsilon)\bar{q}_2, \tag{4.11}$$

$$\bar{r}_o = 2\,\bar{q}_2 \quad , \tag{4.12}$$

$$(c+\varepsilon)\bar{r}_o - d\bar{r}_o/dx + \bar{v}_1 = -\bar{Q}_o \, . \tag{4.13}$$

Substitution of $\bar{r}_o$ and $\bar{v}_1$ in (4.13) from (4.11) and (4.12) yields

$$d\bar{q}_2/dx - 3(c+\varepsilon)\bar{q}_2 = \bar{Q}_o. \tag{4.14}$$

The solution of (4.14) is given by

$$\begin{aligned}
((2n+1)^2(c+\varepsilon)^2+k^2)\bar{q}_{n+1} &= -\frac{k}{c}\left[1+\exp\{2(2n+1)(c+\varepsilon)L\}\right]\exp\{(2n+1)(c+\varepsilon)(x+L)\}, && x<-L,\\
((2n+1)^2(c+\varepsilon)^2+k^2)\bar{q}_{n+1} &= -\frac{1}{c}\left((2n+1)(c+\varepsilon)\cos kx - k\left[\sin kx - \exp\{(2n+1)(c+\varepsilon)(x-L)\}\right]\right), && |x|<L,\\
((2n+1)^2(c+\varepsilon)^2+k^2)\bar{q}_{n+1} &= 0, && x>L,
\end{aligned} \tag{4.15}$$

with n = 1.

Using (3.10), (3.11), (4.11), (4.12), (4.13), (3.9) and (3.25), we may obtain expressions for the transformed variables $\bar{u}$, $\bar{p}$, $\bar{v}$ and $\bar{w}$.

$$\left.\begin{aligned}
\bar{p} &= \tfrac{1}{2}\bar{q}_2\ (1+y^2)\exp(-\tfrac{1}{2}y^2)\\
\bar{u} &= \tfrac{1}{2}\bar{q}_2\ (y^2-3)\exp(-\tfrac{1}{2}y^2)\\
\bar{v} &= \{\frac{1}{c}F(x) + 4(c+\varepsilon)\bar{q}_2\}\, y\, \exp(-\tfrac{1}{2}y^2),\\
\bar{w} &= \tfrac{1}{2}\{\frac{1}{c}F(x) + (c+\varepsilon)\bar{q}_2(1+y^2)\}\exp(-\tfrac{1}{2}y^2).
\end{aligned}\right\} \tag{4.16}$$

The time-dependent solution is obtained by taking the inverse Laplace transform of (4.16). Those who are not interested in the details of the mathematical solution should skip to 3.4(c).

The inverse Laplace transform of $\bar{q}_2(x,c)$ is given by

$$(\gamma^2\varepsilon^2+k^2)\, q_{n+1} = -\Big[\{ke^{\gamma\varepsilon(x+L)} - e^{-\varepsilon t}(\gamma\varepsilon \sin\{k(t/\gamma+(x+L))\} + k\cos\{k(t/\gamma+(x+L))\})\}$$
$$H(t/\gamma+(x+L))$$
$$+ \{ke^{\gamma\varepsilon(x-L)} - e^{-\varepsilon t}(\gamma\varepsilon \sin\{k(t/\gamma+(x-L))\} + k\cos\{k(t/\gamma+(x-L))\})\}$$
$$H(t/\gamma+(x-L))\Big], \quad \text{for } x < -L,$$

$$(\gamma^2\varepsilon^2+k^2)q_{n+1} = -\Big[\gamma\varepsilon\cos kx - k\sin kx - e^{-\varepsilon t}(\gamma\varepsilon\cos\{k(t/\gamma+x)\} - k\sin\{k(t/\gamma+x)\})$$
$$+ \{ke^{\gamma\varepsilon(x-L)} - e^{-\varepsilon t}(\gamma\varepsilon \sin\{k(t/\gamma+(x-L))\} + k\cos\{k(t/\gamma+(x-L))\})\}$$
$$H(t/\gamma+(x-L))\Big], \quad \text{for } |x| < L.$$

$$(\gamma^2\varepsilon^2+k^2)q_{n+1} = 0, \quad \text{for } x > L,$$

where $\gamma = 2n+1$ and $n = 1$. (4.17)

The inverse Laplace transform of $c\bar{q}_2(x,c)$ is given by

$$(\gamma^2\varepsilon^2+k^2)L^{-1}\{c\bar{q}_{n+1}\} = -\gamma\varepsilon e^{-\varepsilon t}\{\sin k(t/\gamma+(x+L))\ H(t/\gamma+(x+L))$$
$$+ \sin k(t/\gamma+(x-L))\ H(t/\gamma+(x-L))\} \text{ for } x < -L,$$

$$(\gamma^2\varepsilon^2+k^2)L^{-1}\{c\bar{q}_{n+1}\} = -\gamma e^{-\varepsilon t}\{\cos k(t/\gamma+x) + \sin k(t/\gamma+(x-L))\ H(t/\gamma+(x-L))\}$$
$$\text{for } |x| < L,$$

$$(\gamma^2\varepsilon^2+k^2)L^{-1}\{c\bar{q}_{n+1}\} = 0 \quad \text{for } x > L.$$

with $\gamma = 2n+1$ and $n = 1$. (4.18)

The solution as a function of x,y,t is found by using (4.17) and (4.18) in the expressions (4.16). The essence of the solution is described by the behaviour of $q_2(x,t)$ and $L^{-1}\{c\bar{q}_2\}$. In terms of these, the solution given by

$$\left.\begin{aligned} p &= \tfrac{1}{2}\, q_2(1+y^2)\, \exp(-\tfrac{1}{4}y^2), \\ u &= \tfrac{1}{2}\, q_2(y^2-3)\, \exp(-\tfrac{1}{4}y^2), \\ v &= \{F(x) + 4(L^{-1}\{c\bar{q}_2\} + \varepsilon q_2)\}\, y\, \exp(-\tfrac{1}{4}y^2), \\ w &= \tfrac{1}{2}\{\, F(x)+(L^{-1}\{c\bar{q}_2\} + \varepsilon q_2)(1+y^2)\}\, \exp(-\tfrac{1}{4}y^2). \end{aligned}\right\} \qquad (4.19)$$

(c) Discussion of the response to symmetric forcing

It is interesting to consider the undamped case $\varepsilon = 0$. Fig. 19(a) shows the amplitude of u (horizontal arrows), p (solid contours) and w (dashed contours) as a function of time at y = 0. First consider the area to the east of the forcing region, where the disturbance is entirely due to the Kelvin wave part (4.8), (4.9). The Kelvin wave is emitted from the forcing region at t = 0 and travels at unit speed (about 40° longitude per day) towards the east, leaving behind it a flow in steady state. The wave front has a width equal to that of the heating region, about 40° of longitude, thus the wave front emerges completely from the heating region in about one day. The complete horizontal structure of the solution is shown in Fig. 20(a). The Kelvin wave part of the circulation to the east of the forcing region is seen to be direct and entirely within the zonal plane. Ascent is confined to the heating region and descent is confined to the wave front. In between, the circulation is completed by low level easterlies and upper level westerlies.

The damped solution for $\varepsilon = 0.1$ is illustrated as a function of time at y = 0 in Fig. 19(b). Fig. 20(b) shows the detailed horizontal structure. Consider again the Kelvin wave part to the east of the forcing region and how it is modified by friction. The propagation speed is not affected, so the time for a steady state to be reached in the heating region depends only on the time for the wave to propagate through, and hence on the size of the region. Between the heating region and the wave front the flow is steady but the amplitude decays exponentially with distance. This is because the amplitude of the disturbance in the wave front region decays like $\exp(-\varepsilon t)$ as the wave front propagates out. In the damped case, the vertical motion is no longer confined to the heating region and the wave front. As in the undamped case, there is ascent in the heating region and descent in the wave front but after the wave front leaves the heating

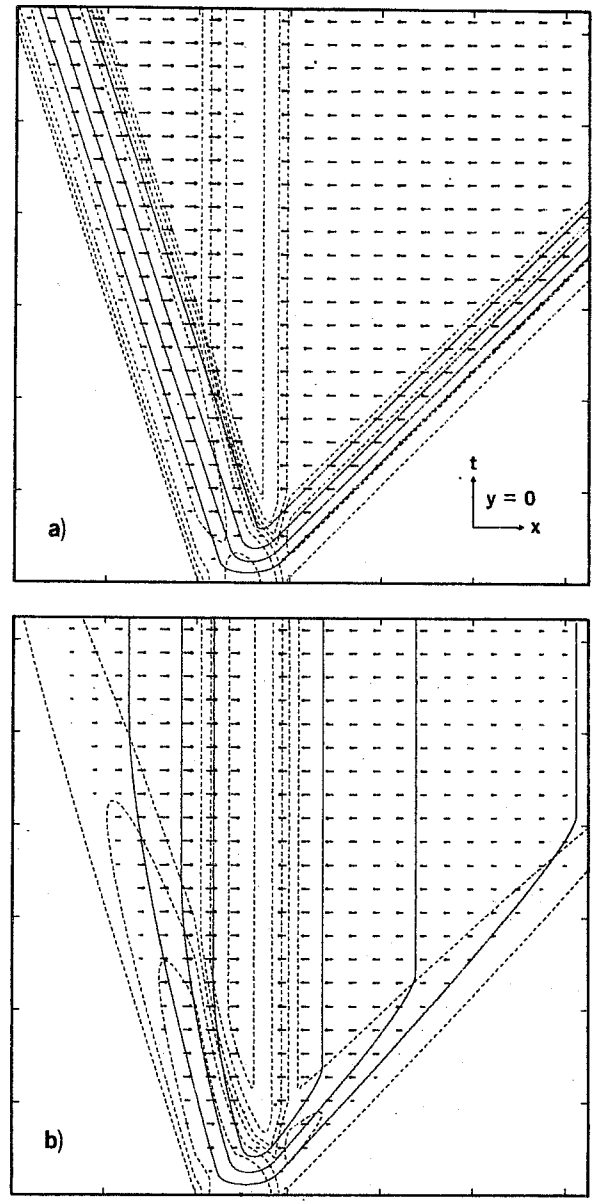

Fig. 19 Response amplitude as a function of time, at y=0, to heating symmetric about the equator localised in the region $|x| < 2$ suddenly switched on at t=0. Solid lines are pressure perturbation, p, contouring interval 0.3. Dashed lines are vertical velocity, w, contour levels ± 0.1 ; $\pm 2^n/10$, $n \geqslant 2$. The horizontal arrows are in the direction of the zonal velocity, u, the length of the arrows are proportional to the logarithm of $|u|$. Both axes are ticked at intervals of four units, corresponding to approximately 1 day for the vertical axis and about 40^o longitude for the horizontal axis. The vertical axis extends from t=0 to t=25. The horizontal axis entends from x=-10 to x=15. (a) The total undamped response (ε=0). (b) The total damped response (ε=0.1).

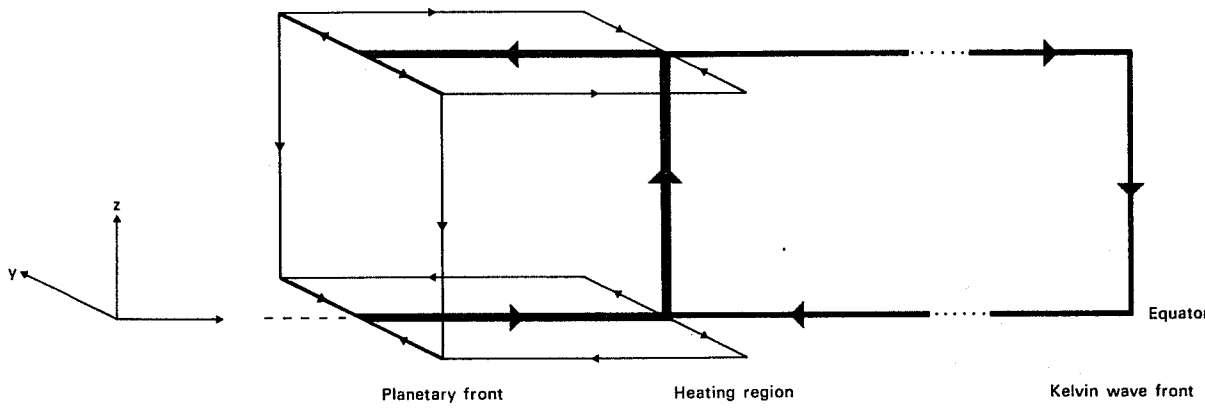

Fig. 21 Schematic illustration of the flow field in the absence of damping.

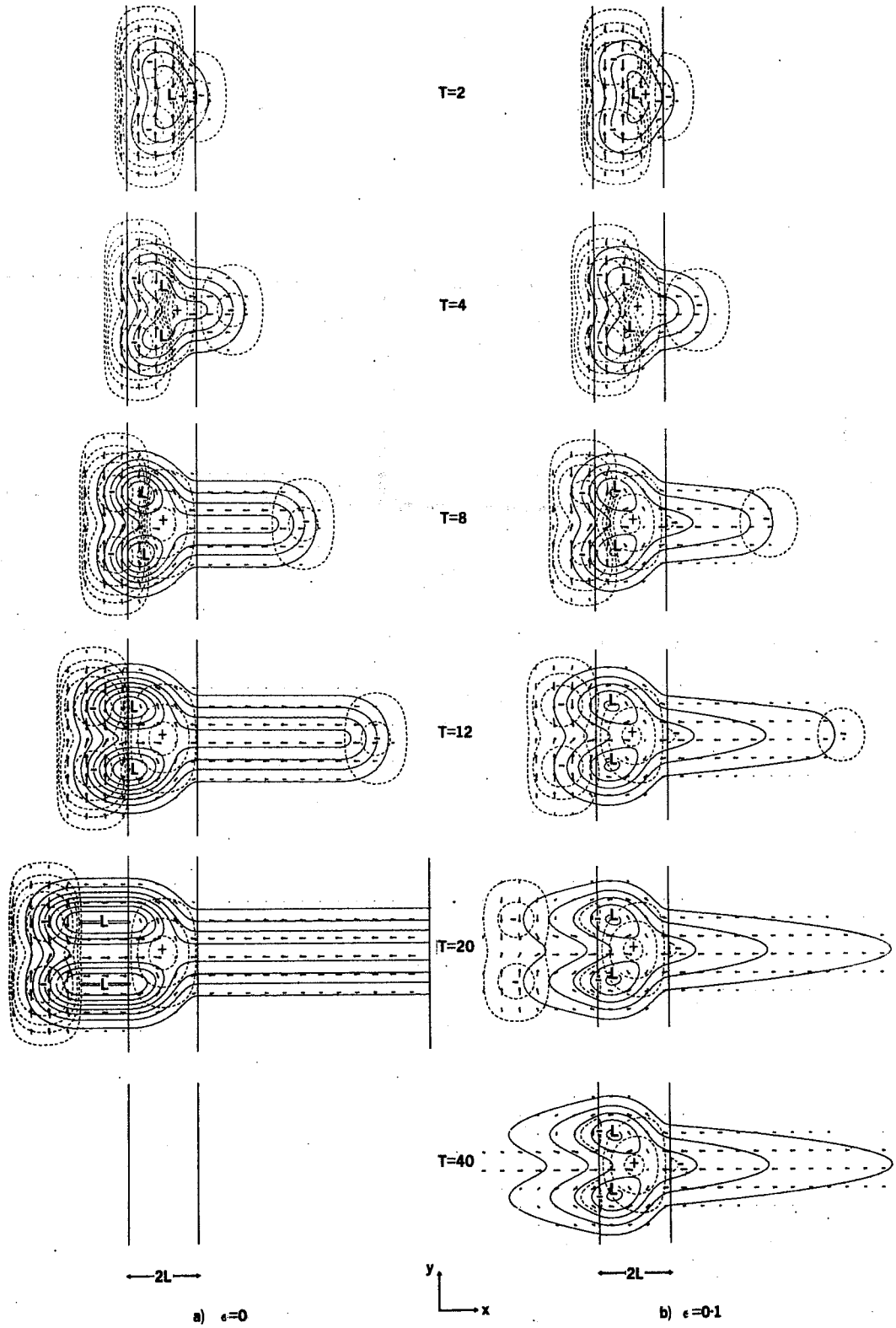

Fig. 20 Total response amplitude as a function of x,y at specific times to heating symmetric about the equator localised in the region $|x| < 2$ suddenly switched on at t=0. Solid lines are pressure perturbation p contouring interval 0.3. Dashed lines vertical velocity w contour levels ± 0.1; $\pm 2^n/10$, $n \geqslant 2$. The horizontal arrows are in the direction of the horizontal velocity, $\underline{v}$, the length of the arrows are proportional to the logarithm of $|\underline{v}| = (u^2+v^2)^{1/2}$. '+' indicates ascent, '-' descent. (a) The undamped case ($\varepsilon=0$). (b) The damped case ($\varepsilon=0.1$).

region a region of relatively strong descent is established immediately adjacent to the heating region on its eastern edge. The magnitude of the vertical velocity in this region decays exponentially with x towards the wave front where the second region of strong descent occurs. Initially the descent is entirely within the wave front, as soon as the wave front leaves the heating region (after about 1 day) the descent begins to be spread over the region between the heating and the wave front reducing the descent within the wave front progressively as it propagates away from the heating until the descent within the wave front is negligable. The circulation at this time consists of ascent within the heating region, descent to the east of the heating region decaying as $\exp(-\varepsilon x)$, low level easterlies and upper level westerlies.

Now consider the area to the west of the forcing region beginning with the undamped case $\varepsilon = 0$ illustrated in Figs. 19(a) and 20(a). Here, the disturbance is entirely due to the planetary wave part (4.19) of the solution. The associated disturbance is emitted from the heating region at $t = 0$ and travels at one third unit speed (about 13^{o} longitude per day) towards the west, leaving behind it a flow in steady state.

The wave front has a width equal to that of the heating region, and so takes about three days to completely emerge from the forcing zone. After the emergence, the circulation that is established has the form shown schematically in Fig. 21 with rising motion in the heating region and low level flow away from the equator, as required by vorticity constraints. ($\beta v = f\partial w/\partial z$). The horizontal flow is cyclonic at low levels and anti-cyclonic at upper levels. In the region of the wave front descent occurs to the north and to the south of the equator with flow towards the equator at low levels and away from it at upper levels; the low level flow is cyclonic and the upper level flow is anti-cyclonic.

The damped solution is shown in Figs. 19(b) and 20(b). The effect of damping on the planetary wave part is similar to that on the Kelvin wave part, with decreasing air spread over the entire region between the wave front and the heating region, and with the descent in the wave front falling off like $\exp(-\varepsilon t)$. Since the wave moves at one-third the Kelvin wave speed, the fall off in amplitude with distance from the forcing region is three times faster than with the Kelvin wave.

3.5 Asymmetric forcing

The heating rate has the form of (3.23), the only non-zero coefficient of $\bar{Q}_n$ is $\bar{Q}_1$ and is given by

$$\bar{Q}_1 = \frac{1}{c} F(x). \tag{5.1}$$

There are, again, two parts to the response. The first part for which (3.18) and (3.19) give

$$\bar{q}_1 = 0, \ \bar{v}_o = \bar{Q}_1, \tag{5.2}$$

corresponds to the long, n=0, mixed Rossby-gravity wave; as pointed out by Gill (1980) and the inverse Laplace transform of which is simply

$$q_1 = 0, \quad v_o = \begin{cases} Q_1 & , \text{ for } t > 0 , \\ 0 & , \text{ for } t < 0 \end{cases} \tag{5.3}$$

which, for $t > 0$, is simply the steady state solution.

The second part of the response is the long, n=2, planetary wave for which (3.18), (3.20) and (3.19) give

$$\bar{v}_2 = \frac{dq_3}{dx} + (c+\varepsilon)\, q_3, \tag{5.4}$$

$$\bar{r}_1 = 3\, \bar{q}_3 \quad , \tag{5.5}$$

$$\frac{d\bar{q}_3}{dx} - 5(c+\varepsilon)\bar{q}_3 = \bar{Q}_1 \ . \tag{5.6}$$

The solution of (5.6) is given by (4.15) with n=2. Using (3.10), (3.11), (5.1), (5.2), (5.4), (5.5), (5.6), (3.25) and (3,9), we may obtain expressions for the transformed variables $\bar{u},\bar{p},\bar{v}$ and $\bar{w}$ in terms of q_3.

$$\left.\begin{aligned} \bar{p} &= \tfrac{1}{2}\, \bar{q}_3\, y^3 \exp(-\tfrac{1}{4}y^2) \quad , \\ \bar{u} &= \tfrac{1}{2}\, \bar{q}_3\, (y^3-6y) \exp(-\tfrac{1}{4}y^2) \quad , \\ \bar{v} &= \{6(c+\varepsilon)\bar{q}_3\, (y^2-1) + \tfrac{1}{c}F(x)y^2\} \exp(-\tfrac{1}{4}y^2), \\ \bar{w} &= \{\tfrac{1}{2}(c+\varepsilon)\bar{q}_3\, y^3 + \tfrac{1}{c}F(x)y\} \exp(-\tfrac{1}{4}y^2). \end{aligned}\right\} \tag{5.7}$$

The time-dependent solution is obtained by taking the inverse Laplace transform of (5.7). The inverse Laplace transform of $\bar{q}_3(x,c)$ is given by (4.17) with n=2, and that of $c\bar{q}_3(x,c)$ is given by (4.18) with n=2. The solution as a function of x,y,t is found by substitution of these inverse transforms in (5.7). In terms of these, the solution is given by

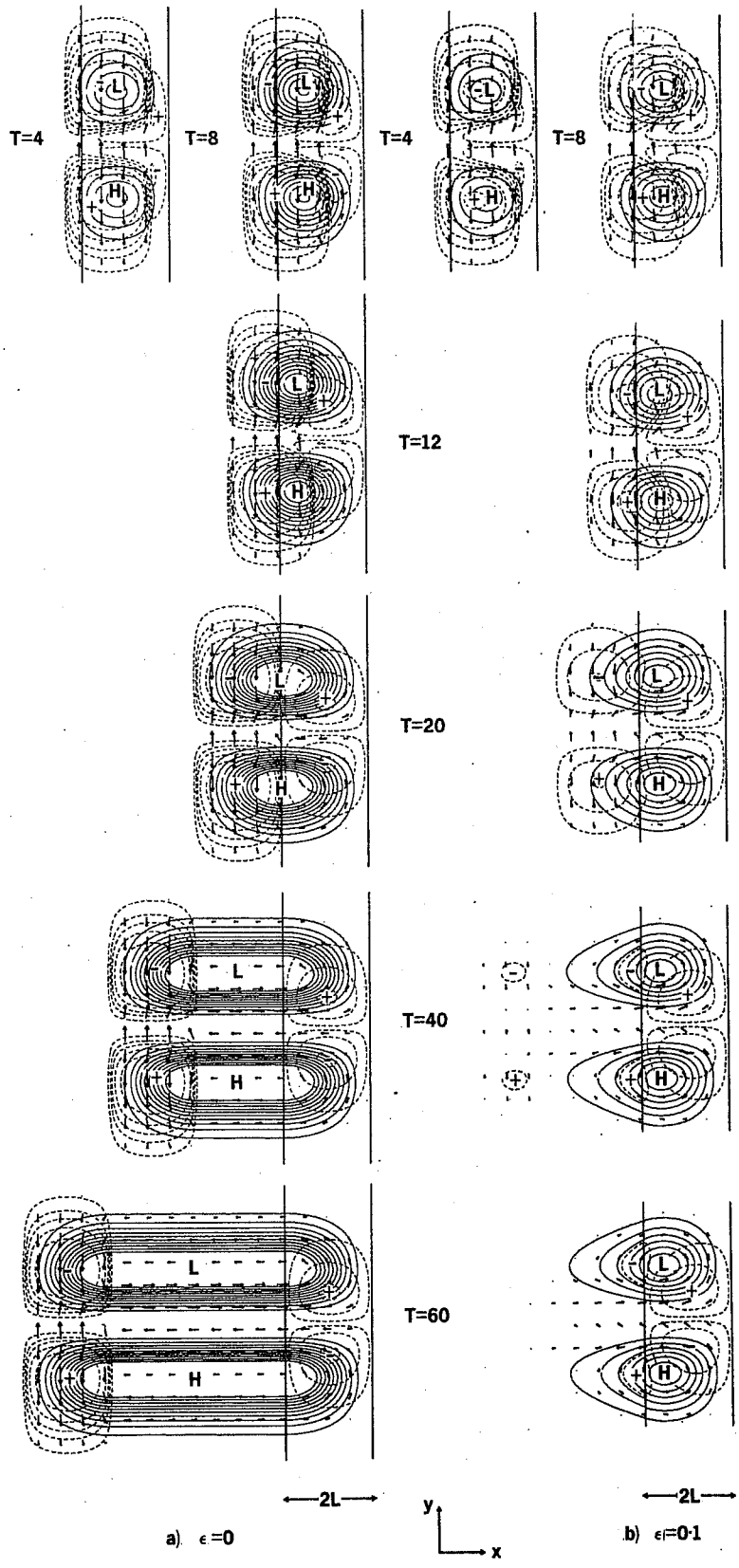

Fig. 22 As Fig. 20 but for the toal response to heating asymmetric about the equator.

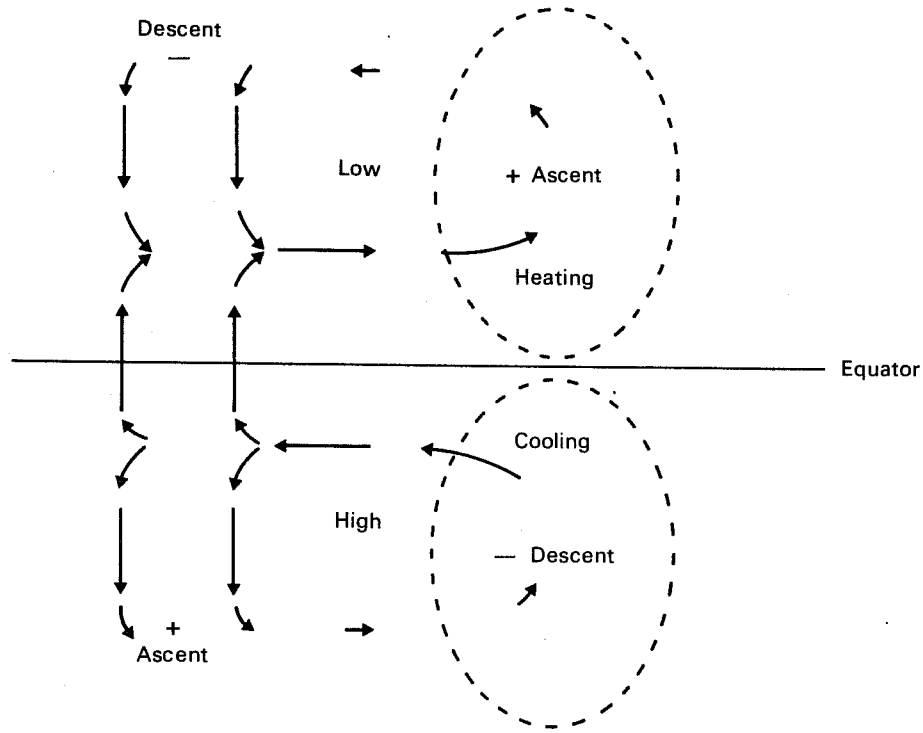

Fig. 23 Schematic illustration of low level flow associated with asymmetric heating.

$$
\left.
\begin{aligned}
p &= \tfrac{1}{2} q_3 \, y^3 \exp(-\tfrac{1}{4}y^2) \quad , \\
u &= \tfrac{1}{2} q_3 \, (y^3-6y) \exp(-\tfrac{1}{4}y^2) \quad , \\
v &= \{ 6 (L^{-1}\{c\bar{q}_3\} + \varepsilon q_3)(y^2-1) + F(x)y^2 \} \exp(-\tfrac{1}{4}y^2) \quad , \\
w &= \{ \tfrac{1}{2}(L^{-1}\{c\bar{q}_3\} + \varepsilon q_3)y^3 + F(x)y \} \exp(-\tfrac{1}{4}y^2) \quad .
\end{aligned}
\right\} \qquad (5.8)
$$

The solution is illustrated in Fig. 22a for the undamped case (ε=0) and in Fig. 24b for the damped case (ε=0.1). The low level flow is illustrated schematically in Fig. 23. The wave front propagates towards the west at one fifth unit speed, about 8° latitude per day. The flow at low levels within the wave front is characterised by a non-divergent southerly cross equatorial flow, northerlies to the north of the equator and southerlies to the south of the equator. The flow is initially dominated by the wave front with a very strong cross equatorial circulation but as the damping takes effect the cross equatorial circulation is steadily weakened until a steady state is finally reached where the circulations in the two hemispheres are almost independent. Once again, we note that the steady state takes a long time to become established. The t=40 (about 10 days) solution is not quite in steady state.

3.6 Vertical structure of solutions

The aim of this study was to present, in an simple a framework as possible, the response of the tropical atmosphere to a sudden 'switch-on' of a heat source. Attention has been concentrated on the horizontal structure of the solutions which were found only for a single vertical mode. As pointed out by Gill (1980), this single vertical mode is the complete solution for an incompressible atmosphere with constant buoyancy frequency N, a rigid lid at Z=D, and for which the diabatic heating varies as $\sin(\pi Z/D)$, in which case u,v and p vary as $\cos(\pi Z/D)$ with w varies as $\sin(\pi Z/D)$. This representation of the solution is a useful aid to understanding and has been used to obtain the schematic illustrations in the text.

4. DISCUSSION

As has been demonstrated by Haseler (1982), the tropical circulations can significantly influence the extratropical flow in the medium range. Unfortunately, experience shows that the tropical flow is very difficult to predict. Investigations of monthly means of forecasts show errors within the first 24 hours of up to 7 or 8 ms^{-1} in the wind field at 850 mb and up to 11 or 12 ms^{-1} at 150 mb. These errors continue to grow, although more slowly, for on average 7 to 8 days. Such large errors occurring in the quasi-stationary flow suggests problems associated with stationary forcing, i.e. orography or large scale heating. Close examination of the flow field associated with the tropical errors reveals a surprisingly simple structure. The errors are largely associated with the South American and African continents with Africa being the dominant source of error. The erroneous flow in the African region consists, on the large scale, of easterlies off West Africa, westerlies off East Africa and anti-cyclonic flow over North and South Africa. The mean error in the low level flow is the reverse of this with westerlies off West Africa, easterlies off East Africa and cyclonic flow over North and South Africa. As shown in section 3, this flow pattern is precisely what one would expect for a heat induced tropical circulation where the heat source is symmetric about the equator and corresponds to an eastward travelling, damped, Kelvin wave and a westward travelling, damped, symmetric Rossby wave. The structure of the flow revealed in theoretical studies and the timescales involved agree with the evolution of the error field in the forecasts, suggesting that a substantial part of the forecast errors in the tropics are associated with erroneous large scale heating at the start of the forecast. This result does not exclude orography as a source of error since, for example, incorrect extrapolation of pressure data over high orography would essentially appear as a spurious thermal source in the analysis. An obvious candidate for these errors in the adiabatic non-linear normal mode initialisation. The absence of diabatic forcing in the initialisation results in an initial data set for the model with very little tropical divergence. Starting a forecast from an adiabatically initialised data set is like switching on a heat source. After the switch-on the model rapidly "spins up". Recent incorporation of the diabatic processes in the analysis has resulted in only a modest improvement in the forecasting of the tropical wind field. Another possible candidate is the

absence of a diurnal cycle in the forecasting system. There are large diurnal and semi-diurnal variations in near surface parameters, the semi-diurnal pressure tide is particularly strong in the tropics. The model, which provides the first guess for the analysis, does not simulate the semi-diurnal tide and therefore the first guess pressure field in the tropics can disagree with observations by up to a few mb according to the phase of the tide. The observational network over Africa consists mainly of a few SYNOP stations and the 12Z observations coincide with a peak in the tide. This surface pressure data is accepted by the analysis scheme resulting in temperature increases at low levels of several degrees which produces an analysis with a very unstable vertical stratification. On starting a forecast this instability is released in the form of very intense convection. Unrealistically large precipitation increases the soil moisture over the African continent which, in turn, allows the enhanced convection to become established; this could permanently change the model's large scale thermal forcing and hence the model's tropical climatology.

It is expected that a correct accounting for the diurnal cycles in the data will result in substantially improved tropical forecasts.

Acknowledgements

Many people have contributed to this work in the form of useful discussions and the provision of computer programs. In particular I should like to thank Tony Hollingsworth for suggesting the study, Werner Wergen for providing the programs to compute the normal modes and Adrian Gill for helpful discussions on the correct interpretation of the analytical solutions.

REFERENCES

Abramowitz, M. and Stegun, I.A. 1965 Handbook of Mathematical Functions, Dover, 1046 pp.

Gill, A.E. 1980 Some simple solutions for heat-induced tropical circulation. Quart. J.R. Met. Soc., 106, 447-462.

Haseler, J. 1982 An investigation of the impact at middle and high latitudes of tropical forecast errors. ECMWF Technical Report No. 31, 42 pp. Available from the European Centre for Medium Range Weather Forecasts, Reading, England.

Hollingsworth, A. and Simmons, A.J. 1983 A note on Gill's simple solutions for heat-induced tropical circulations. To appear as ECMWF Technical Report. Available from the European Centre for Medium Range Weather Forecasts, Reading, England.